AN ABSTRACT OF THE THESIS OF

CHUJYH CHANG for the degree of Master of Science in Electrical and Computer Engineering presented on October 5, 1989.

Title: MODELING AND CHARACTERIZATION OF HEMT DEVICES

Abstract approved: Redacted for Privacy

Stephen M. Goodnick

Different gate length (0.5 μm - 16 μm) AlGaAs/GaAs and AlGaAs/InGaAs High Electron Mobility Transistors were electrically characterized in order to compare the room temperature DC device performance with one-dimensional device models. Model parameters such as the channel mobility and source/drain series resistances are extracted from independent measurement of the source-drain conductance characteristics. Using the saturated velocity as a fit parameter to the current voltage characteristics, good agreement with the expected value of this quantity is found in the two different systems.

MODELING AND CHARACTERIZATION OF HEMT DEVICES

by

Chujyh Chang

A THESIS

Submitted to

Oregon State University

in partial fulfillment of
the requirements for the
degree of

Master of Science

Completed October 5, 1989

Commencement June 1990

APPROVED:

Redacted for Privacy

Professor of Electrical and Computer Engineering in Charge of major

Redacted for Privacy

Head of Department of Electrical and Computer Engineering

Redacted for Privacy

Dean of C

Date thesis is presented October 5, 1989

ACKNOWLEDGEMENTS

I would like to give special thanks to my major professor, Prof. Stephen M. Goodnick, for his patient guidance throughtout my thesis at OSU. I wish to thank Prof. Sayfe Kiaei, my minor professor, for his guidance. Special thanks to Prof. David Allstot and Prof. Alan Love for acting as my committee members and for giving me useful advice. I would also like to thank Bruce Odekirk at Triquint Semiconductor, Beaverton OR, for providing the samples for my research.

I would like to take this opportunity to thank my parents and family members for their financial support and encourage, without which I would not have been able to come to the USA for my study.

TABLE OF CONTENTS

1. Introduction 1
1.1 The High Electron Mobility Transistor 1
1.2 Structure of the HEMT 2
1.3 Relative Advantages And Disadvantages 4
1.4 Pseudomorphic HEMTs (AlGaAs/InGaAs HEMTs) 5
1.5 Goal of Present Research 7

2. 1D Models of HEMT 10
2.1 The Band Diagram 10
2.2 Energy Levels In The Potential Well 11
2.3 Interface Sheet Carrier Concentration 15
2.4 Charge Control 17
2.5 Analytical Models of HEMT 19
2.5.1 2DEG Transport Properties 19
2.5.2 Two-piece Model 20
2.5.3 Exponential Model 22

3. Experimental 33
3.1 Material Growth And Device Fabrication 33
3.2 Characterization 34

4. Results 40
4.1 Device Performance 40
4.1.1 Drain Current 41
4.1.2 Transconductance 41
4.1.3 Saturation Current 42
4.2 Device Characteristics 42
4.2.1 Threshold Voltage And Mobility 43
4.2.2 Source and Drain Series Resistance 45
4.3 Fits Model Using The Exponential Model 46

5. Discussion of Results 70

Bibliography 75

Appendix I 2DEG Concentration Program 78

Appendix II I-V Characteristics Program 80

LIST OF FIGURES

Figure | **Page**

1.1 Cross section of a typical HEMT structure 8

1.2 Flowchart of my research 9

2.1 Band diagram of AlGaAs/GaAs heterojunction 26

2.2 Interface carrier density n_{so} vs. doping density with the undoped AlGaAs layer thickness d_i as a parameter 27

2.3 Conduction band edge diagram of a single period modulation doped structure with a Schottky barrier deposited on the AlGaAs layer 28

2.4 Channel potential versus distance along the gate of a high electron mobility field effect transistor 29

2.5 Comparison of the empirical models and experimental results for the electron drift velocity as a function of electric field for AlGaAs/GaAs at 300K. The data is from Masselinket al.[14] The curve of equ. (2.38) assumes that μ = 9000 cm^2/Vsec; υ_s = 8 x 10^6 cm/sec 30

2.6 Flowchart of I-V curve fitting routine 31

2.7 Comparison of I-V Curves for the two-piece model and the exponential model 32

3.1 Epitaxial layers for H100 36

3.2 Layer Structure of H108 37

3.3 Layout of the HEMTs 38

3.4 Measurement system for DC device characterization 39

4.1 I-V curves of H100 (L = 0.5 μm) 50

4.2 I-V curves of H100 (L = 8 μm) 51

4.3 I-V curve of H108 (L = 0.5 μm) 52

4.4 I-V curve of H108 (L = 8 μm) 53

4.5 Transconductance at function of gate voltage for H100 54

4.6 Transconductance at function of gate voltage for H108 55

4.7 Saturation current at function of gate voltage for H100 56

4.8 Saturation current at function of gate voltage for H108 57

4.9 Total conductance at function of gate voltage (H100, L=2 mm) 58

4.10 Total resistance of the H100 59

4.11 Total resistance of the H108 60

4.12 "end" resistance measure technique 61

4.13 "end" resistance measurement for the H100 62

4.14 "end" resistance measurement for the H108 63

4.15 Saturation current vs. gate length at different gate bias for H100 64

4.16 Saturation current vs. gate length at different gate bias for H108 65

4.17 Theoretical and experimental I-V curves for H100 (L = 0.5 μm) 66

4.18 Theoretical and experimental I-V curves for H100 (L = 8 μm) 67

4.19 Theoretical and experimental I-V curves for H108 (L = 0.5 μm) 68

4.20 Theoretical and experimental I-V curves for H108 (L = 8 μm) 69

5.1 Improvement in assuming optimized values for Rs, Rd, and μ at 300 K I-V curves for H100 (L = 8 μm) 74

LIST OF TABLES

Table	Page
4.1 The threshold voltage for samples H100 and H108	48
4.2 The thickness of the doped AlGaAs layer for samples H100 and H108 calaulated from the threshold voltage data, Table 4.1	49
5.1 The measurement physical parameters for samples H100 and H108	73

MODELING AND CHARACTERIZATION OF HEMT DEVICES

1. Introduction

1.1 The High Electron Mobility Transistor

A high electron mobility transistor (HEMT) is a heterojunction device which takes advantage of the high electron mobility and carrier drift velocity of the two-dimensional electron gas (2DEG) which resides at a lattice matched heterointerface or strained layer, typically between $Al_xGa_{1-x}As$ and undoped GaAs or $In_xGa_{1-x}As$. Through the technique of modulation-doping discussed in more detail later, extremely high carrier mobility may be realized which is interesting both for device applications and for the study of two-dimensional effects in semiconductor systems. Since the first demonstration of enhanced mobility structures in 1978,[1] research in the area of high electron mobility transistors (HEMTs), (also called selectively doped heterojunction transistors (SDHTs) and modulation doped field effect transistors (MODFETs)) has progressed rapidly in the 1980s.

In 1960, R.A. Anderson first predicted that an accumulation layer may appear at the interface of a heterojunction.[2] Later, In 1969, L. Esaki and R. Tsu suggested that the mobility of the two-dimensional electron gas at such an interface could be improved through spatial separation of impurities from the heterointerface.[3] In

1978, R. Dingle et al.[1] were the first to observe an enhanced electron mobility of the two-dimensional electron gas. In 1980, T. Mimura et al.[4] fabricated the first heterojunction field effect transistor which utilized the mobility enhancement of the two-dimensional electron gas. Since then, a number of groups have fabricated devices and circuits with impressive results.

HEMTs offers new possibilities for high-speed, low-power, large scale integration. A historical account of the reduction in gate delay time and the race to the 10 psec barrier has been given by R. Dingle et al.[5] There, a comprehensive summary is given of a number of HEMT SSI circuits which have successfully been demonstrated which include:

a) Ring oscillators.

b) Static RAM's.

c) Frequency dividers.

d) 8 x 8 bit parallel multiplier.

e) Voltage comparator.

f) 2-20 GHz distributed amplifier.

1.2 Structure of The HEMT

HEMT structures with enhanced mobility have now been grown using liquid phase epitaxy (LPE), metal-organic chemical vapor deposition (MOCVD), and molecular beam epitaxy (MBE). The basic HEMT structure, shown in Fig. 1.1, consists of four distinct layers. These layers are usually referred to as the channel layer (layer

A), the undoped spacer layer (layer B), the donor layer (layer C), and the cap layer (layer D). The physical purpose of each layer is as follows: An active channel is formed on the top surface of the undoped GaAs buffer layer that is grown on a semi-insulating GaAs substrate. Typically this layer thickness is approximately 1 μm. On top of the active channel, a thin layer (typically, 20 Å to 60 Å) of undoped $Al_xGa_{1-x}As$, called the "setback" or "spacer", is grown. Since this layer is undoped, it further separates the channel electrons from the donor impurities residing in the doped $Al_xGa_{1-x}As$ layer. While an increased thickness of this layer enhances the electron mobility, it also results in lower electron densities in the channel which is undesirable. Above the "spacer layer" is the doped $Al_xGa_{1-x}As$ layer which supplies the electrons for channel conduction and acts as a high-quality dielectric material between the gate and the two- dimensional electron gas. As in silicon, it is the high quality of the AlGaAs/GaAs interface (equivalent to low Q_{ss} on the Si/SiO_2 interface) that makes high-performance HEMT operation possible. The HEMT structure is capped by a layer of highly doped GaAs which passivates the $Al_xGa_{1-x}As$ and facilitates ohmic contact to the 2DEG.

The flexibility of MBE crystal growth allows the HEMT designer a wide variety of device options. Some variations of the HEMT structure included inverted structures, n+ GaAs gate HEMTs, p+ GaAs gate HEMTs and insulated gate HEMTs. In the present work, we will concentrate only on the normal structure shown in Fig. 1.1.

1.3 Relative Advantages and Disadvantages

Both the MESFET and the HEMT are field-effect transistor (FET) in which the electron concentration in the channel between the source and drain is modulated by the gate voltage. Because of the higher electron mobility and peak velocity in the III-V compound semiconductors as compared to that in Si, the speed advantage for GaAs over Si has long been recognized. However, in a MESFET, ionized donor impurities resides in the channel which reduces the mobility and drift velocity due to scattering.

In contrast, for HEMTs, the electrons which transfer from the wider bandgap $Al_xGa_{1-x}As$ to the narrow bandgap GaAs are confined to the undoped GaAs layer. This layer has a much greater mobility and drift velocity than in the case of doped GaAs due to the spatial separation resulting from modulation doping which should make HEMTs intrinsically faster than MESFETs.

However, due to the high quality of the critical layers needed in HEMT fabrication, precise crystal-growth methods are needed such as molecular beam epitaxy (MBE) or metal-organic chemical vapor deposition (MOCVD) which allow growth of heterolayers with extremely sharp interfaces. Hence, one of the main disadvantages of HEMTs is in the cost of fabrication as well as the cost of substrate materials (III-V compounds) which are more expensive than silicon technology. In spite of the high performance of HEMT devices, a number of problems must be overcome for HEMTs to compete in the

commercial IC market. These problems include light sensitivity, threshold voltage variation, and instability in the I-V characteristics. When exposed to light at low temperature (< 140 K), the selectively doped AlGaAs/GaAs heterojunction exhibits a photocurrent that continues even after the light source is removed,[6] referred to as the persistent photoconductivity effect (PPC). For photon energies higher than the AlGaAs bandgap, the main cause of PPC seems to be electron photoexcitation from the deep traps in the n-type AlGaAs donor layer.[7] These deep traps are most likely donor-defect complexes, referred to as the DX centers in the study by D.V. Lang et al.[8] Another serious problem, I-V instability, is observed at cryogenic temperature in complete darkness. When the drain bias is above a certain threshold, the drain I-V curves distort, giving the appearance of a forward-bias junction diode in series with the drain. This is the so-called "I-V collapse"[9] which occurs independent of gate bias, is also believed to be related to the DX centers.[10]

1.4 Pseudomorphic HEMTs (AlGaAs/InGaAs HEMTs)

A new type of HEMT using the AlGaAs/InGaAs heterojunction structure has been recently introduced to help alleviate some of the trapping problems observed in GaAs/AlGaAs. InGaAs, which is lattice mismatched to GaAs, can be grown sufficiently thin so that the mismatch is accommodated entirely as elastic strain.[11] Under such conditions, the interface between the AlGaAs and the InGaAs is

essentially free from misfit dislocation and the thin layer of InGaAs is said to be pseudomorphic.

The larger conduction band offset of the AlGaAs/InGaAs system compared to that of the AlGaAs/GaAs system makes it possible to reduce the Al mole fraction in the $Al_xGa_{1-x}As$ donor layer, and thus greatly reduce the DX center concentration and the problems associated with them. Pseudomorphic HEMTs employing such a layer exhibit no PPC or I-V collapse phenomena at reduced temperatures,[12] and have superior low frequency noise characteristics.[13] Also, the saturation velocity of InGaAs is significantly higher than that of GaAs. The saturation velocities for the $Al_{0.3}Ga_{0.7}As/GaAs$ structure[14] and the lattice matched $In_{0.52}Al_{0.48}As/In_{0.53}Ga_{0.47}As$ structure[15] have been measured as 8×10^6 cm^2/sec and 2×10^7 cm^2/sec, respectively. Therefore, assuming we can linearly interpolate between the values of GaAs and InAs, a formula for the saturation velocity in $In_xGa_{1-x}As$ may be written (assuming a negligible effect due to strain)

$$\upsilon_s\,(In_xGa_{1-x}As) = ((1.2\,x/0.53) + 0.8)10^7 \qquad (1.1)$$

where x is In mole fraction in the $In_xGa_{1-x}As$. Typical mole fractions in pseudomorphic HEMTs range from 0.1 - 0.25. Thus an improvement of as much as 70.75 % may be realized in the saturated velocity.

1.5 Goal of Present Research

The objectives of the present research are to compare the measured DC device characteristics of variable gate length AlGaAs/GaAs HEMTs and AlGaAs/InGaAs pseudomorphic HEMTs to one-dimensional device models. From parameter fits between theory and experiment, we obtain the saturated drift velocities of the two systems, which are compared to the theoretically expected values as given by equation (1.1) in order to test the validity of the 1D models.

In chapter 2, we discuss one-dimensional device models of HEMTs which are later used to fit the experimental I-V characteristics. In chapter 3, we discuss the material growth and device fabrication of the samples which were studied. In chapter 4, we discuss the DC device performance including the I-V curves characteristics, the transconductance, and saturation current. There, we obtain the model parameters such as the threshold voltage, Rs, Rd, and μ from the measured DC characteristics. Finally, we obtain υ_S from model fits to the I-V curves which is discussed in Chapter 5. The research plan in my thesis is shown in Fig. 1.2.

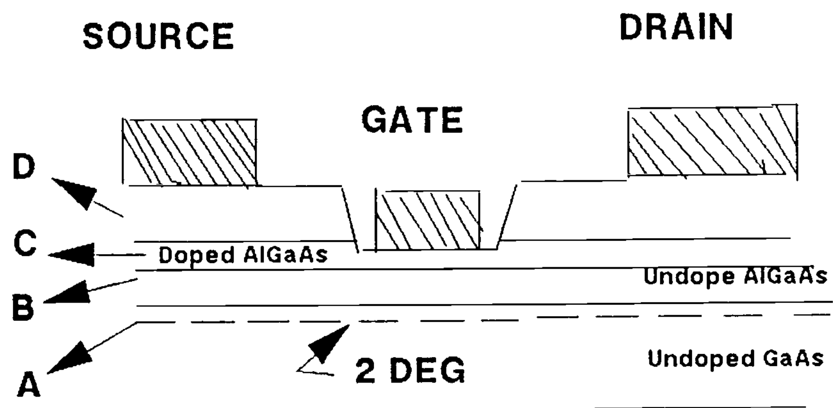

Figure 1.1 Cross section of a typical HEMT structure.

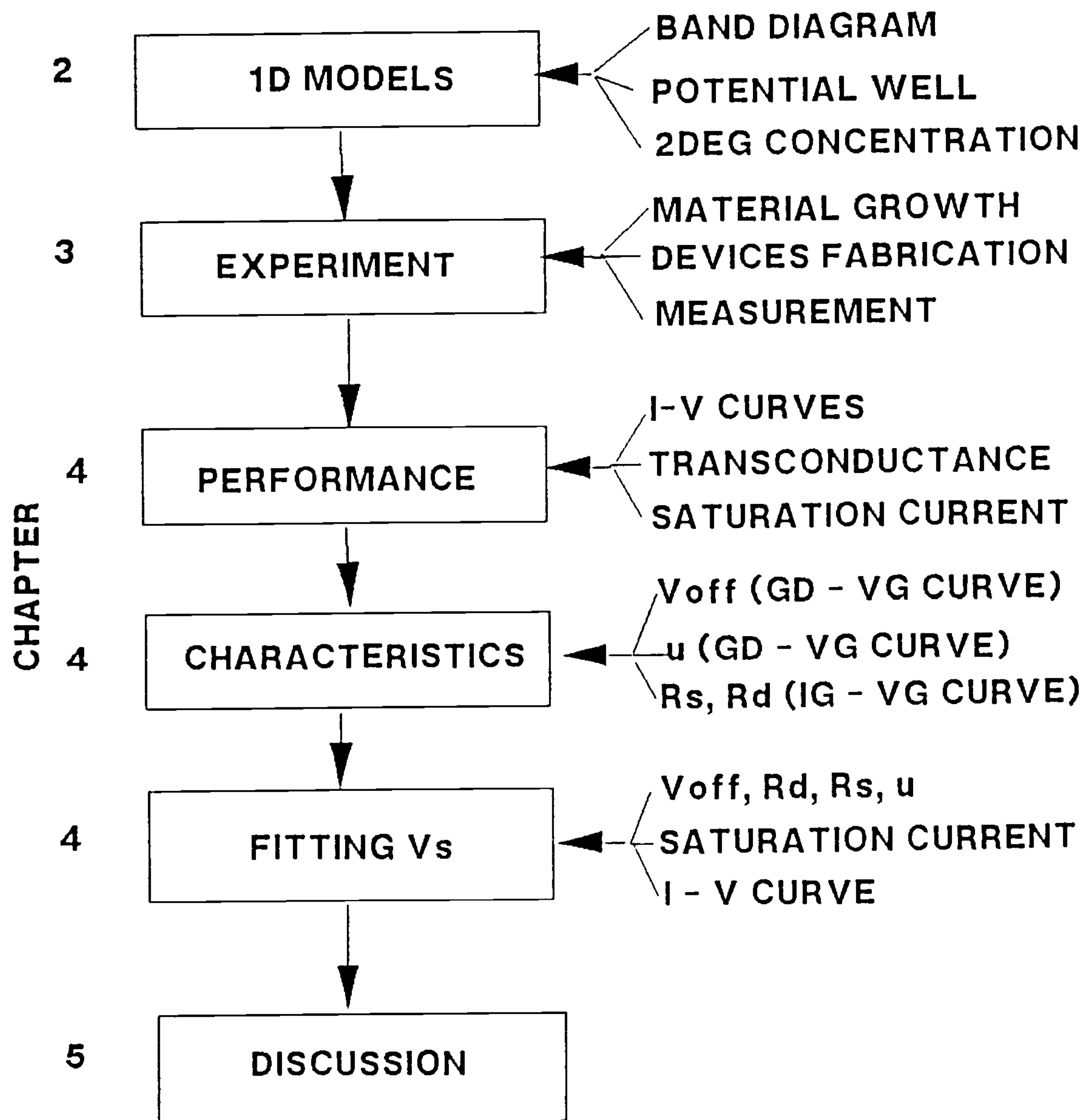

Figure 1.2 Flowchart of my research.

2. 1D MODELS OF HEMTS

This chapter discusses the electron energy band diagram and the relationship between the 2DEG carrier concentration and the various potentials existing in the device. First, we calculate the maximum interface sheet density at equilibrium as a function of AlGaAs doping concentration and device dimensions. From this we proceed to derive a basic one-dimensional device model of the HEMT.

2.1 The Band Diagram

One of the characteristic features of a heterojunction is the discontinuity in the electronic and material properties which occurs at the interface between the two dissimilar materials. When a high band gap semiconductor (such as $Al_xGa_{1-x}As$) is grown on a lower band gap semiconductor (such as GaAs or $In_xGa_{1-x}As$), the difference in the two band gaps will be accommodated partially as an offset in the conduction and the valence band edges. In the AlGaAs/GaAs system, about 67% of the difference in the bandgap between the two species occurs in the conduction band, corresponding essentially to the electron affinity difference between the materials, and the remaining 33% occurs in the valence band.[16] In the case of the strained $Al_yGa_{1-y}As$ (y = 0.2-0.35) - $In_xGa_{1-x}As$ (x = 0.12-0.35) interface, the conduction band offset is believed to be 60% to 75% of

the bandgap difference, although there still exists significant discrepancy in the experimentally measured values.[17]

Alignment of the Fermi level in equilibrium requires that electrons diffuse from the $Al_xGa_{1-x}As$ to the undoped layer. Thus an accumulation of electrons results at the interface between the two materials which forms a two-dimensional electron gas (2DEG) with a width on the order of a few tens of angstroms. The 2DEG localized near the heterojunction and the ionized donors in the $Al_xGa_{1-x}As$ give rise to a strong electric field, which in turn causes pronounced band bending, particularly in the GaAs, as shown in Fig. 2.1 for a single period modulation-doped AlGaAs/GaAs heterojunction .

An important effect is the parasitic MESFET effect which occurs when the doped AlGaAs layer is no longer depleted. In this case of incomplete electron transfer to the quantum well channel, electron states in both channel and barrier will be occupied. Thus the conductivity will consist of both parallel conduction in the channel and barriers which degrades device performance for large gate biases as discussed in Section 4.1.2.

2.2 Energy Levels In The Potential Well

In order to determine the 2DEG carrier concentration, n_{so}, we need to know the relationship between the 2DEG carrier concentration and the various energy levels. As shown in the band diagram (Fig. 2.1) for the heterojunction, a potential minimum for electrons exists at the interface in the narrow gap semiconductor

which results in spatial confinement of electrons in the well. Quantum mechanically, such carrier confinement in a quantum well results in the formation of discrete energy levels called subbands which are the eigenvalues of the time independent Schrodinger's equation in one dimension discussed in more detail below. For the AlGaAs/GaAs system, the lowest two subbands account for 80-90 % of sheet charge density for most of the attainable densities.[18] The existence of the 2DEG has been demonstrated by measuring the angular dependence of the magnetoresistance, where it has been observed that the magnetic field induced (Shubnikov-de Haas) conductance oscillations depend only on the component of the magnetic field perpendicular to the interface.[19] The periodicity in the Shubnikov-de Haas oscillations can be used to calculate the quantized energy levels and the sheet carrier density.[6]

To calculate the subband energies, one must solve the Schrodinger equation in one dimension

$$\frac{h^2}{2m^*}\frac{d^2\psi}{dx^2} + (E_i - V(x))\psi = 0 \qquad (2.1)$$

where V(x) represents the one-dimensional potential associated with the variation of the conduction band edge shown in Fig. 2.1 due to the band offset and the potential arising with ionized donors in the AlGaAs.

An appropriate approximation to the potential, V(x), allows analytic solutions of (2.1) to be found. Usually, the potential is assumed to be given by a triangular approximation

$$V(x) = \infty\ ,\ x \leq 0 \qquad (2.2.a)$$

$$V(x) = q\, E_0\, x\ ,\ x > 0 \tag{2.2.b}$$

where E_0 is the electric field at the interface. The assumption of an infinite interface potential implies that the penetration of the wave function into the AlGaAs is neglible. The solutions to equation (2.1) are the Airy functions[20]

$$\psi_i = A_i \left\{ \frac{2m^* q E_0^{1/2}}{h^2} \left(x - \frac{E_i}{q E_0} \right) \right\} \quad i = 0,1,2,\ldots,n \tag{2.3}$$

where E_i is the ith energy eigenvalue given approximately by[21]

$$E_i = \left(\frac{h^2}{2m^*} \right)^{1/3} \left(\frac{3}{2} \pi q E_0 \right)^{2/3} \left(i + \frac{3}{4} \right)^{2/3}. \tag{2.4}$$

For GaAs, E_0 and E_1 are

$$E_0 = 1.83 \times 10^{-6}\ E_0^{2/3} \tag{2.5.a}$$

$$E_1 = 3.23 \times 10^{-6}\ E_0^{2/3} \tag{2.5.b}$$

where the energy is measured in electron volts. The interface carrier concentration can be related to the subband energies if it is expressed in terms of the electric field. To do that, Poission's equation must be solved

$$dE/dx = -qn(x)/\varepsilon_1 \tag{2.6}$$

where $n(x)$ and ε_1, are the free electron concentration and the dielectric constant in the narrow bandgap material respectively. Integration within the depletion region results in (Gauss' Law)

$$\varepsilon_1\, E_0 = q\, n_s \tag{2.7}$$

where ε_1 and n_s are the interface electric field and carrier concentration respectively. Using equations (2.5) and (2.7)

$$E_0 = \lambda_0\, (n_{so})^{2/3} \tag{2.8.a}$$

$$E_1 = \lambda_1 (n_{so})^{2/3} \tag{2.8.b}$$

where λ_0 and λ_1 may be solved from the above equations. However, in practice these constants are treated as adjustable parameters used to yield a good agreement with experiments. Using the experimental Shubnikov-de Haas results[6], the factors appearing in equation (2.8) have been estimated as[22]

$$\lambda_0 = 2.5 \times 10^{-12} \; (Jm^{3/4}) \tag{2.9.a}$$

$$\lambda_1 = 3.2 \times 10^{-12} \; (Jm^{3/4}). \tag{2.9.b}$$

The density of states for a single quantized level in two dimensions is given by

$$D = \frac{m^*}{\pi h^2} \tag{2.10}$$

which from the measured cyclotron mass is given by

$$D = 3.24 \times 10^{17} \; (m^{-2} \, eV^{-1}). \tag{2.11}$$

For electrons with energies above the second level E_1 either subband may be occupied and the equivalent density of states equals 2D. The total number of electrons may be determined using the Fermi Dirac distribution

$$n_{so} = D \int_{E_0}^{E_1} \frac{dE}{1 - \exp\left(\frac{E - qV(d_i+)}{KT}\right)} + 2D \int_{E_1}^{\infty} \frac{dE}{1 + \exp\left(\frac{E - qV(d_i+)}{KT}\right)}. \tag{2.12}$$

Solving the integral yields

$$n_{so} = \frac{DKT}{q} \log\left[\left(1 + \exp\left(\frac{qV(d_i+) - E_0}{KT}\right)\right)\left(1 + \exp\left(\frac{qV(d_i+) - E_1}{KT}\right)\right)\right] \tag{2.13}$$

where the bottom of the conduction band $qV(d_i^+)$ represents the Fermi level. Under equilibrium, the charge depleted from the larger

bandgap material must equal the interface charge density. A solution is then found such that the Fermi level is constant across the heterostructure.

2.3 Interface Sheet Carrier Concentration

The expression for the sheet carrier concentration of the AlGaAs/GaAs or AlGaAs/InGaAs interface assuming the depletion approximation holds is given by the following[22]

$$qn_{so} = -qN_d d_i + \sqrt{q^2 N_d d_i + 2\varepsilon_2 V_{20} q N_d} \tag{2.14}$$

where

N_d = Doping concentration in the donor layer

ε_2 = dielectric constant in the donor layer

V_{20} = band bending in the AlGaAs layer of the interface at equilibrium with no gate bias

d_i = undoped spacer layer thickness.

It has been recognized that for typical doping densities, the depletion approximation solution is not accurate enough.[23] The reason for this inaccuracy is that the electron gas in AlGaAs is nearly degenerate, leading to a smaller space charge at the edge of the depletion layer. This reduction in space charge results in a smaller electron interface density and interface electric field than predicted by the depletion approximation. Lee and Shur[23] derived the expression for the 2DEG concentration of AlGaAs/GaAs interface using the full expression for the occupancy of donor states and free electron concentration instead of assuming full depletion as following

$$n_{so} = \sqrt{\frac{2\varepsilon_2 N_d}{q}[-V(d_i+)+V(-W_2)+\delta+N_d^2 d_i^2]} - N_d d_i \quad (2.15)$$

where

δ = correction to the band bending in the AlGaAs layer

$V_{20} = -V(d_i^-) + V(-W_2)$ (total band bending in AlGaAs layer

$V(-W2)$ = the difference between the Fermi level and the bottom of the conduction band edge away from the heterojunction

d_i^- = the coordinate corresponds to the $Al_xGa_{1-x}As$ side of the heterojunction.

From above equations, we solve equation (2.15) with equation (2.13) in which n_{so} is expressed in terms of the density of states, D, and the two lowest energy levels in the potential well in GaAs as described earlier in equation (2.8). The result for the AlGaAs/GaAs interface for the case of x = 0.3 (Al mole fraction in AlGaAs) for different 2DEG concentrations is shown as a function of AlGaAs doping at T = 300K in Fig. 2.2. The Fortran program for calculating the 2DEG concentration is shown in Appendix I. From Fig. 2.2, we observe that when the spacer layer becomes thicker, the 2DEG concentration in the AlGaAs/GaAs interface becomes smaller due to the spacer layer hindering the transfer of the electrons from the doped AlGaAs to the quantum well in the GaAs.

A very accurate analytical approximation to the exact computer solution may be obtained if equation (2.13) is linearized with respect to $V(d_i+)$[23]

$$-E_{Fi}/q = \Delta E_{F0}(T)/q + a\, n_{so}\,, \quad (V(d_i^+) \text{ as } E_{Fi}/q) \quad (2.16)$$

where a = 0.125E-16(V m^2) and ΔE_{FO} = 0 at 300K and ΔE_{FO} = 0.025 at 77K and below. Using equation (2.15) leads to the following simple formula for n_{so}[23]

$$n_{s0} = \sqrt{\frac{2\varepsilon_2 N_d}{q}} \sqrt{\left[\frac{\Delta E_c + \Delta E_{F0}(T)}{q} + \delta + V(-W_2) + N_d^2 (d_i + \Delta d)^2 \right]} - N_d (d_i + \Delta d) \quad (2.17)$$

where effective 2DEG channel width $\Delta d = \varepsilon\, a/q$ = 80 Å, and ΔE_c is the conduction band discontinuity between the two different materials at the interface.

2.4 Charge Control

In order to derive a model for the HEMT current-voltage characteristics, we must derive an expression relating n_s to the applied gate bias. In a HEMT structure, the band diagram with a Schottky barrier gate is shown in Fig. 2.3. The electrostatic potential in such a case can be calculated by integrating the electric field versus distance. This integration, assuming the doped $Al_xGa_{1-x}As$ layer is totally depleted, gives

$$V_2 = qN_d\, d_d^2/2\varepsilon_2 - E_2(0)d \quad (2.18)$$

where $d = (d_d + d_i)$ and

$$qn_s = \varepsilon_2\, E_2(d_i-) = \varepsilon_2\, E_2(0) = \varepsilon_2\, (V_{p2}-V_2)/d \quad (2.19)$$

where

$$V_{p2} = qN_d\, d_d^2/2\,\varepsilon_2 \quad (2.20)$$

is the voltage necessary to pinch off the doped $Al_xGa_{1-x}As$ layer , d_d is the thickness of the doped $Al_xGa_{1-x}As$, d_i is the thickness of the spacer layer, E_2 is the electric field in the $Al_xGa_{1-x}As$ layer as shown

in Fig. 2.1, d_d is the doped concentration of the $Al_xGa_{1-x}As$ layer and ε_2 is the dielectric constant of the doped $Al_xGa_{1-x}As$ layer. From Fig. 2.3 it is apparent that

$$V_2 = \Phi_b - V_G + (E_{Fi} - \Delta E_c)/q \tag{2.21}$$

where Φ_b is the Schottky barrier height, V_G is the applied gate voltage, and E_{Fi} is the fermi level. Combining equations (2.19) and (2.21) leads to

$$n_s = \varepsilon_2 [V_G - (\Phi_b - V_{p2} + E_{Fi}/q - \Delta Ec/q)/(qd). \tag{2.22}$$

We know that $-V(d_i+)$ is a function of n_s by equation (2.16). Replacing E_{Fi}/q by the linearized expression (2.16), the charge is finally given by

$$Qs = qn_s = \varepsilon_2 (V_G - V_{off})/(d + \Delta d) \tag{2.23}$$

where

$$V_{off} = \Phi_b - \Delta E_c - V_{p2} + \Delta E_{F0}(T)/q \tag{2.24}$$

is the "off voltage" which corresponds to the threshold voltage of the 2DEG, Δd is the 2DEG channel width, $\Delta E_{F0} = 0$ at 300K and $\Delta E_{F0} = 0.025$ at 77 K and below. From the equation (2.24), we know the threshold voltage is controlled by several factors: the Schottky barrier height, the conduction band discontinuity of the heterojunction, the doping concentration of AlGaAs, and the thickness of the doped AlGaAs layer under the gate. Φ_b, the Schottky barrier height and ΔE_c, the conduction band discontinuity are related to fundamental material parameters such as the mole fraction of Al. The doping concentration in the AlGaAs, N_d, and the thickness of the doped AlGaAs layer, d_d, are related to device fabrication parameters. Depletion-mode (or normally-on) devices correspond to devices turned on at $V_G = 0$ V,

while enhancement-mode (or normally-off) devices turned for $V_G > 0$ V. Therefore, adjustment of the threshold voltage, V_{off}, is one of the most critical process steps in the HEMT process.

2.5 Analytical Models Of HEMT

2.5.1 2DEG Transport Properties

The electron mobility, μ, is the key parameter of the two-dimensional electron gas (2DEG) that is influenced by growth parameters and layer design. It can be directly related to HEMT device characteristics. Since the electrons and donors are spatially separated, ionized impurity scattering is substantially reduced, making it possible to obtain extremely high electron mobilities. This effect has been calculated in detail by Price[24] and Ando[25]. Other mobility mechanisms to be considered are interface roughness and intersubband transitions. Mori and Ando also considered interface roughness in the calculations.[26] Stormer et al. have considered intersubband scattering and have apparently been able to observed the effect in devices.[27]

At high fields, the carrier drift velocity is no longer proportional to the electric field due to carrier heating effects. The saturated drift velocity is the most important parameter in characterizing the speed performance of short channel FET devices, since the characteristic delay is inversely proportional to υ_S. The saturation velocities for the $Al_{0.3}Ga_{0.7}As/GaAs$ structure[14] and the lattice matched $In_{0.52}Al_{0.48}As/In_{0.53}Ga_{0.47}As$ structure[15] have

been measured as 8×10^6 cm^2/sec and 2×10^7 cm^2/sec, respectively.

2.5.2 Two-piece Model

A two-dimensional cross section of a HEMT structure is illustrated in Fig. 2.4. The AlGaAs layer in a HEMT is fully depleted under normal operating conditions and the electrons are confined to the heterointerface. Application of a drain voltage in addition to the gate voltage gives rise to a potential distribution varying from zero at the source end to V_D' at the drain. The 2DEG density, assuming the gradual channel approximation, depends on the gate voltage, V_G, and the potential, $V_c(x)$, in the 2DEG channel according to following equation

$$Q_s(x) = \varepsilon_2 (V_G - V_c(x) - V_{off})/(d + \Delta d) \qquad (2.25)$$

where ε_2 is the permittivity of $Al_xGa_{1-x}As$, $d = d_d + d_i$ is the thickness of total $Al_xGa_{1-x}As$ layer, $V_c(x)$ is the channel potential and V_{off} is the threshold voltage from the equation (2.24). The drain current is given by

$$I_D = Qs(x)\, Z\, \upsilon(x) \qquad (2.26)$$

where Z is the gate width and $\upsilon(x)$ is the electron drift velocity. Now we will use a two piece linear approximation for the velocity field characteristic as shown in Fig. 2.5. Mathematically

$$\upsilon = \mu E, \quad E < Ec \qquad (2.27.a)$$

$$\upsilon = \upsilon_s, \quad E > Ec \qquad (2.27.b)$$

where μ is the low field mobility, υ_S is the saturated velocity, and E_c is the critical field. At fields less than E_c, we obtain

$$I_D = \{\mu Z \varepsilon_2 (V_G - V_c(x) - V_{off}) dV_c/dx\} / (d + \Delta d) \tag{2.28}$$

where $dV_c/dx = E$ is the electric field.

For the case where $E < E_c$, we obtain a current-voltage characteristics using integration of equation (2.28) at drain voltages less than the saturation voltage

$$I_D = \{(V_G - V_{off})V_D - V_D^2/2\}\{\varepsilon\mu Z/\{(d+\Delta d)L\}\}. \tag{2.29}$$

If the series resistance can't be neglected, equation (2.28) is integrated using

$$V_c(x = 0) = Rs\ I_D \tag{2.30}$$

$$V_c(x = L) = V_D' = V_D - (Rd+Rs)\ I_D \tag{2.31}$$

where Rs and Rd denote the source and drain resistance. As we increase the drain voltage, the electric field near the drain end at x = L will reach the critical value first, called E_c;

$$E(x)|_{x=L} = E_c = (I_S/\beta L)[(V_G' - Rs\ I_S)^2 - 2I_S/\beta]^{-1/2} \tag{2.32}$$

where

$$\beta = \mu\ \varepsilon_2\ Z/[(d + \Delta d)L]\ ,\ V_G' = V_G - V_{off} \tag{2.33}$$

and Is is the saturation current. Solving for Is leads to[28]

$$Is = \frac{\beta V_{SI}^2}{(1-\beta Rs V_G')^2}\left[\sqrt{\left[1+2\beta Rs V_G' + \left(\frac{V_G'}{V_{SI}}\right)^2\right]} - (1+\beta Rs V_G')\right] \tag{2.34}$$

where $V_{SI} = E_c L$.

For short channel devices, V_{SI} can be small compared to V_G' and the expression for Is can be reduced to

$$I_S = \varepsilon_2\ Z\ \upsilon_S\ V_G'/(d + \Delta d). \tag{2.35}$$

The transconductance in the saturation region is

$g_m|_{max} = \partial I_S/\partial V_G |_{V_D'} = \varepsilon_2 Z \upsilon_s/(d + \Delta d).$ (2.36)

For long channel device, using equation (2.34)

$$g_m = \frac{\partial Is}{\partial V_G} = \beta \frac{V_G'}{\sqrt{1 + \left(\frac{V_G'}{V_{SI}}\right)^2}} \quad . \tag{2.37}$$

The advantange of the two-piece models is the simple, closed form expressions for g_m and I_S. The disadvantage of this model is the use of a discontinuous velocity-field which results in discontinuous I-V characteristics calculated using this model.

2.5.2 Exponential Model

In order to improve the agreement between theory and experiment, we have concluded a more sophisticated model for the velocity-field dependence using the empirical formula [29]

$\upsilon(E) = \upsilon_S$ (1 - exp (1 - $\mu E/\upsilon_S$). (2.38)

As can be seen from Fig. 2.5, the exponential model fits the experimental data better than the 2-piece model. Equation (2.38) will be used here to derive an analytical model of I-V characteristics for HEMTs.

The drain current is again given by equation (2.26). Now, substituting from equations (2.38) and (2.25) into (2.26) gives the following equation

$I_D = G_0 (V_G - V_c(x) - V_{off}) (1- \exp(-\mu\, E/\upsilon_S))$ (2.39)

where V_{off} is the threshold voltage and

$G_0 = q^2\, \varepsilon_2/(q^2(d_d+d_i) + \varepsilon_2\, qa).$ (2.40)

From $E = dV_C/dx$, equation (2.39) becomes

$$\frac{dV(x)}{dx} = -\frac{\upsilon_S}{\mu}\ln\left\{1-\frac{I_D}{G_0(V_G-V_{off}-V_C(x))}\right\} . \tag{2.41}$$

Integrating the equation from x= 0 to x= L yields

$$\int_{V_C(0)}^{V_C(L)} \frac{dV}{\ln\left(1-\frac{I_D}{G_0(V_G-V_{off}-V_C(x))}\right)} = -\frac{\upsilon_S L}{\mu} \tag{2.42}$$

and

$$V_C(0) = I_D\, Rs \tag{2.43.a}$$

$$V_C(L) = V_D - I_D\, Rd. \tag{2.43.b}$$

Let

$$t(x) = \frac{I_D}{G_0(V_G-V_{off}-V_C(x))} . \tag{2.44}$$

Equation (2.42) becomes[30]

$$I_D\int_{t_0}^{t_L}\frac{dt}{t^2\ln}\frac{1}{(1-t)} = -\frac{\upsilon_S L G_0}{\mu} \tag{2.45}$$

where

$$t_0 = t(0) = \frac{I_D}{G_0(V_G-V_{off}-I_D Rs)} \tag{2.46.a}$$

$$t_L = t(L) = \frac{I_D}{G_0(V_G-V_{off}-V_D+I_D R_D)} . \tag{2.46.b}$$

From equation (2.45), we can obtain transconductance, $g_m = dI_D/dV_G$, and channel conductance, $g_D = dI_D/dV_D$, as follows

$$g_m = \frac{\ln(1-t_L)-\ln(1-t_0)}{\left[V_G-V_{off}+\frac{\upsilon_S L}{\mu}\ln(1-t_0)\right]\ln(1-t_L)-(V_G-V_{off}-V_D)\ln(1-t_0)} \tag{2.47}$$

$$g_D = \frac{I_D \ln(1-t_0)}{\left[V_G - V_{off} + \frac{\upsilon_S L}{\mu}\ln(1-t_0)\right]\ln(1-t_L) - (V_G - V_{off})\ln(1-t_0)} \quad . \qquad (2.48)$$

In saturation, the channel conductance is equal to zero and thus from equation (2.48), one can obtain

$$t_{L,SAT} = \frac{I_{D,SAT}}{G_0(V_G - V_{off} - V_{D,SAT} + I_{D,SAT} R_D)} = 1 \quad . \qquad (2.49)$$

From equation (4.42) - (4.46), the solutions for this model of the I-V characteristics is obtained by numerical integration. As shown in Fig. 2-6, the procedure is as follows:

a) Input the material parameters and measured device parameters (e.g. N_d, d_d, μ, etc.).

b) Start with drain current I_D equal to 10^{-6} A. From equation (4.46), we obtain the t_L and t_0. Then we integrate the left hand side of the equation (4.45) using a traperzoidal rule.

c) If the value of integration is not equal to the right hand side the estimated root is chosen using the newton method and equation (4,45) is integrated again until we find the root ID.

d) When $t_L = 1$, the drain current goes into the saturation region. ($I_D = I_{DS}$)

The Fortran program for calculating the I-V characteristics is shown in Appendix II. From the Fig.2-7, we can see the comparison I-V curves of the exponential model and the two-piece model. In the low drain voltage region, the I-V curves of the exponential model and the two-piece model are the same. When drain voltage approaches the velocity saturation region, the current of two-piece model at low

gate bias is higher than the current of exponential model, while at the high gate bias, the current of the exponential model is higher. As shown in Fig. 2.7, the two-piece model results in a discontinuity in the I-V characteristic at the transition from the ohmic region to the saturation region due to the discontinuous approximation to the velocity-field dependence.

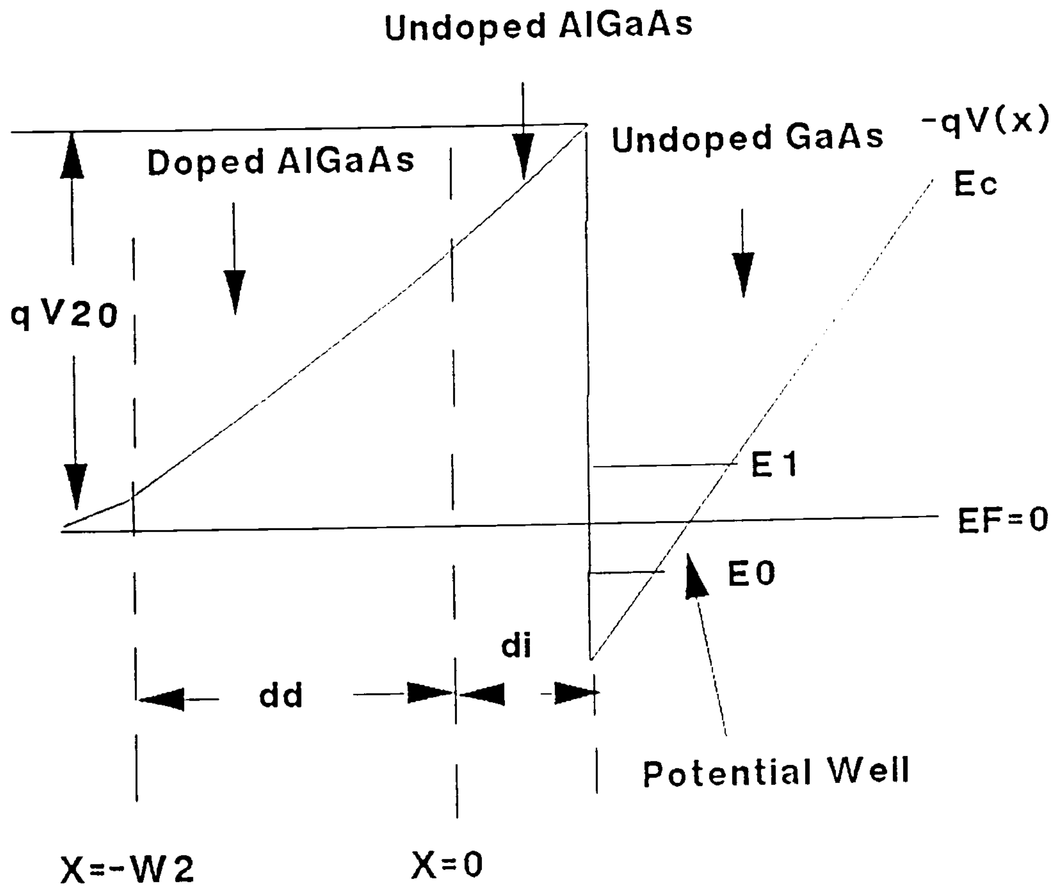

Figure 2.1 Band diagram of AlGaAs/GaAs heterojunction.

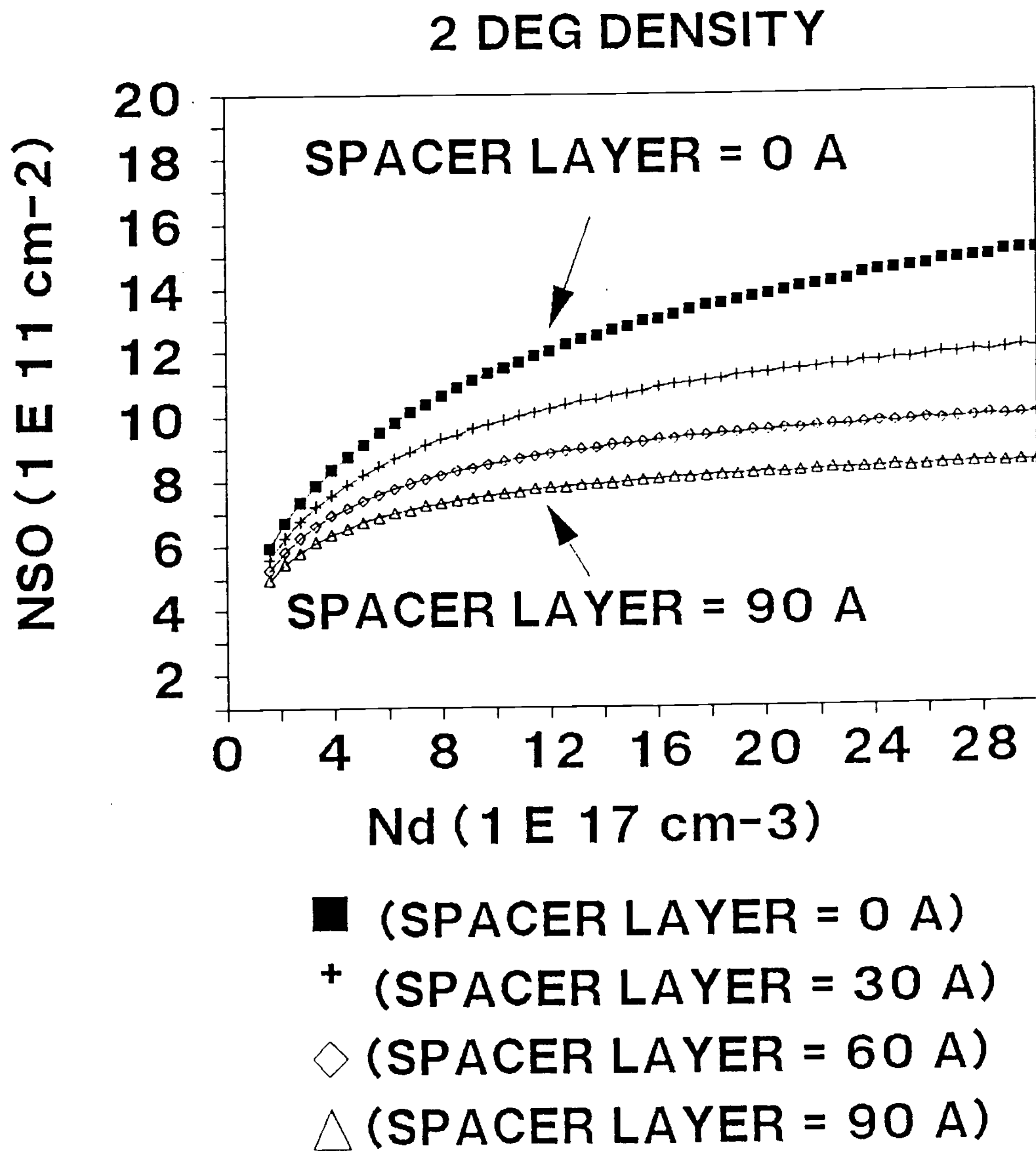

Figure 2.2 Interface carrier density n_{so} vs doping density with the undoped AlGaAs layer thickness d_l as a parameter.

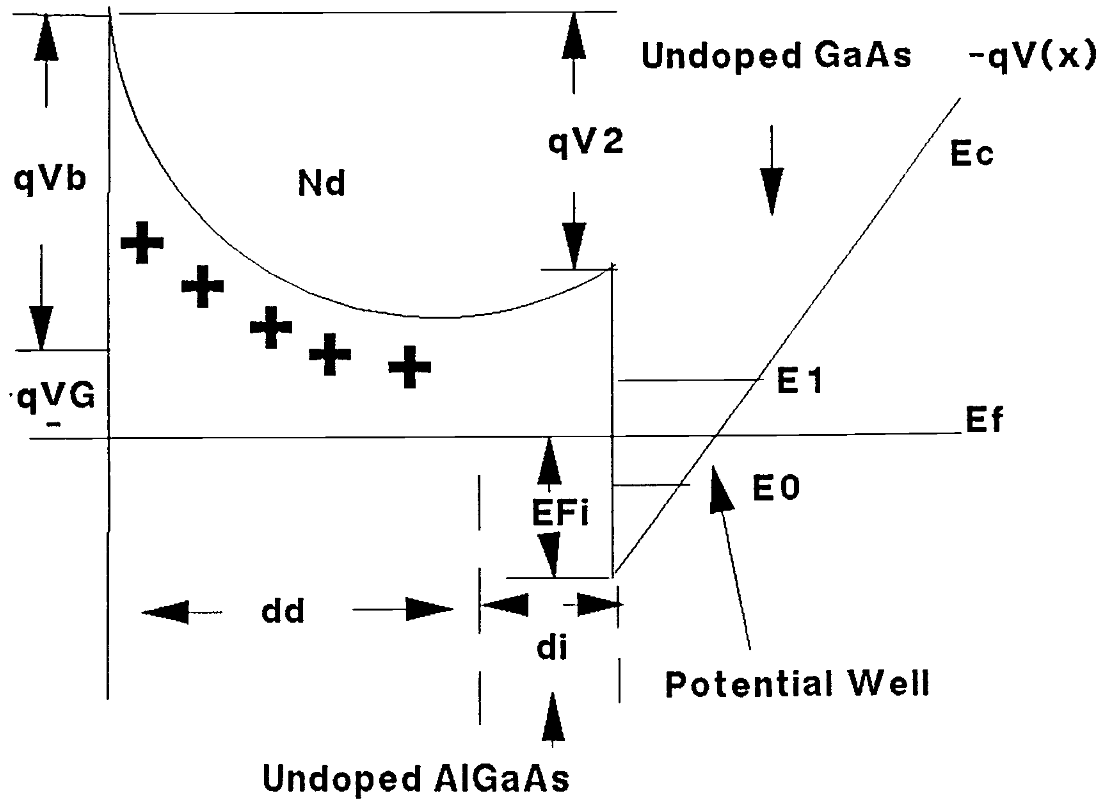

Figure 2.3 Conduction band edge diagram of a single period modulation doped structure with a Schottky barrier deposited on the AlGaAs layer.

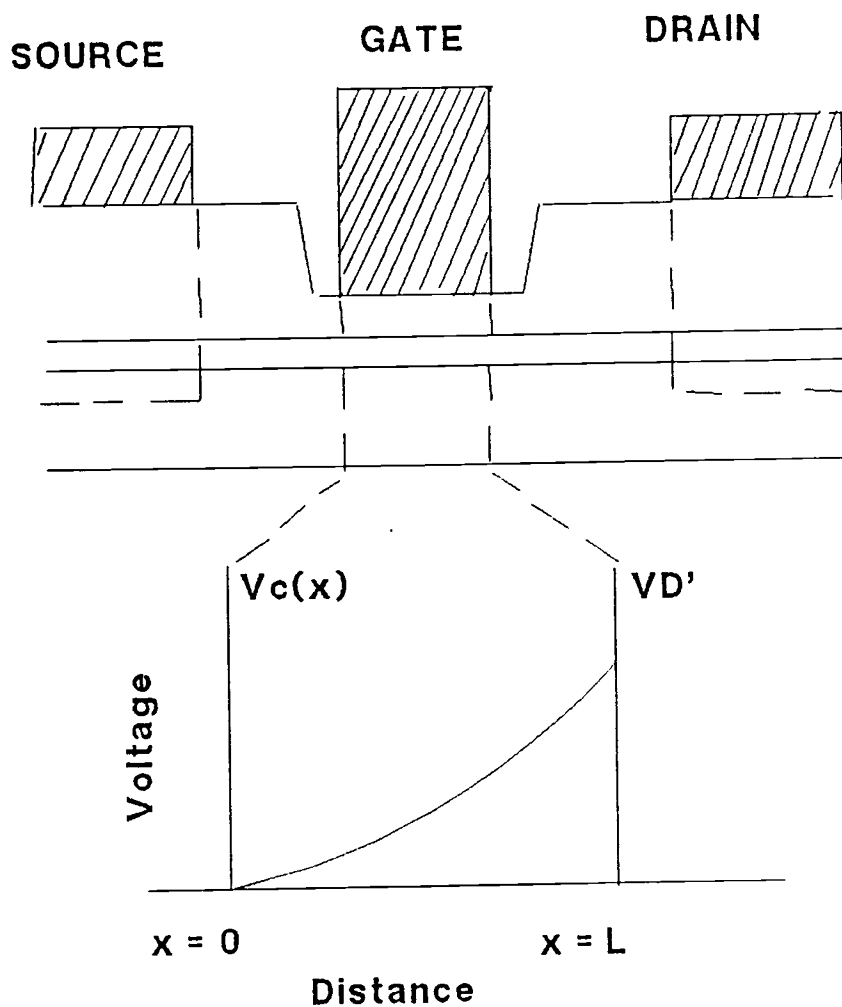

Figure 2.4 Channel potential versus distance along the gate for a high electron mobility field effect transistor.

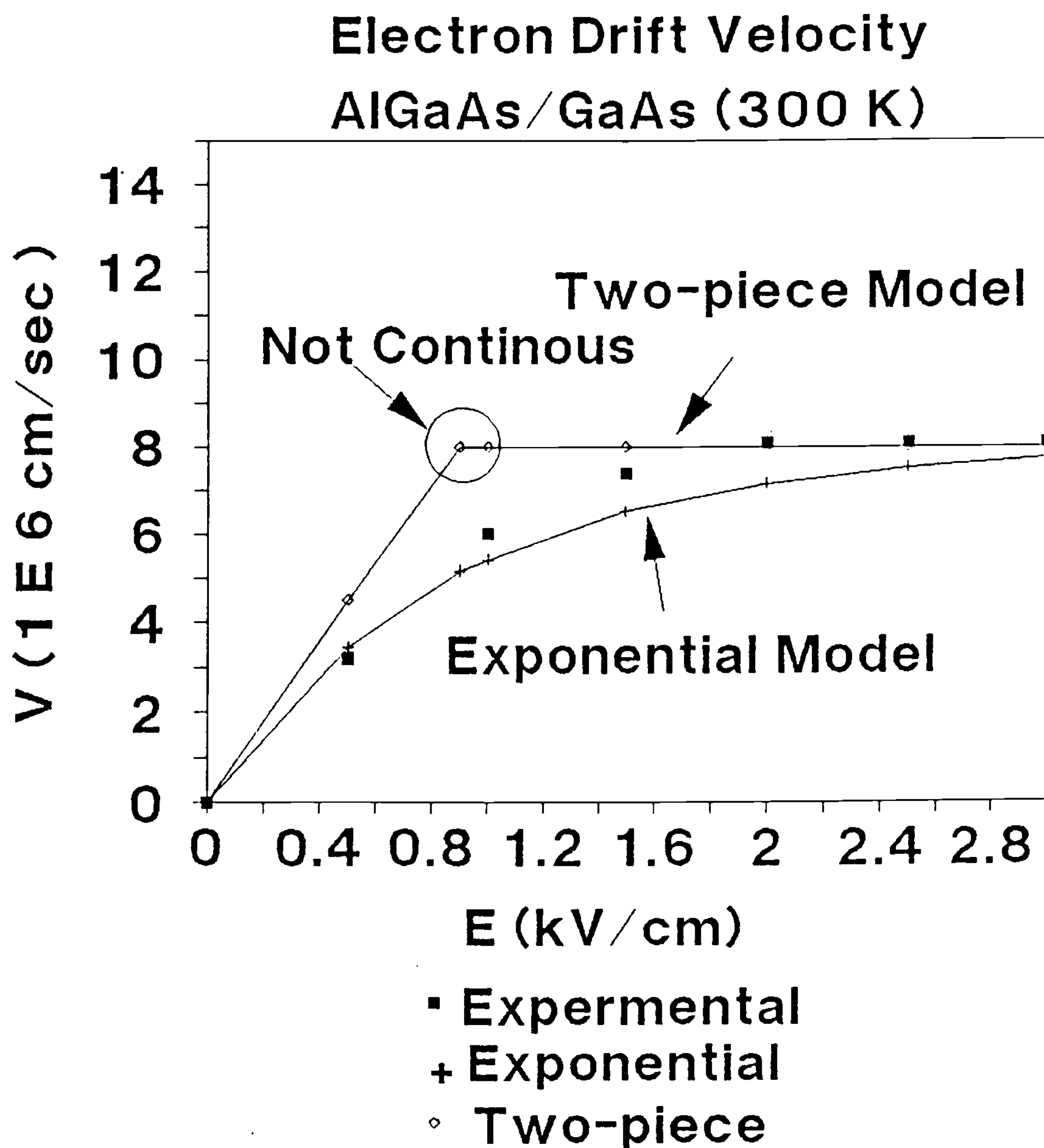

Figure 2.5 Comparison of the empirical models and experimental results for the electron drift velocity as a function of electric field for AlGaAs/GaAs at 300K. The data is from Masselink et al.[14]: the curve for (2.38) assuming that μ = 9000 cm^2/v.sec and vs = 8 X 10^6 cm/sec.

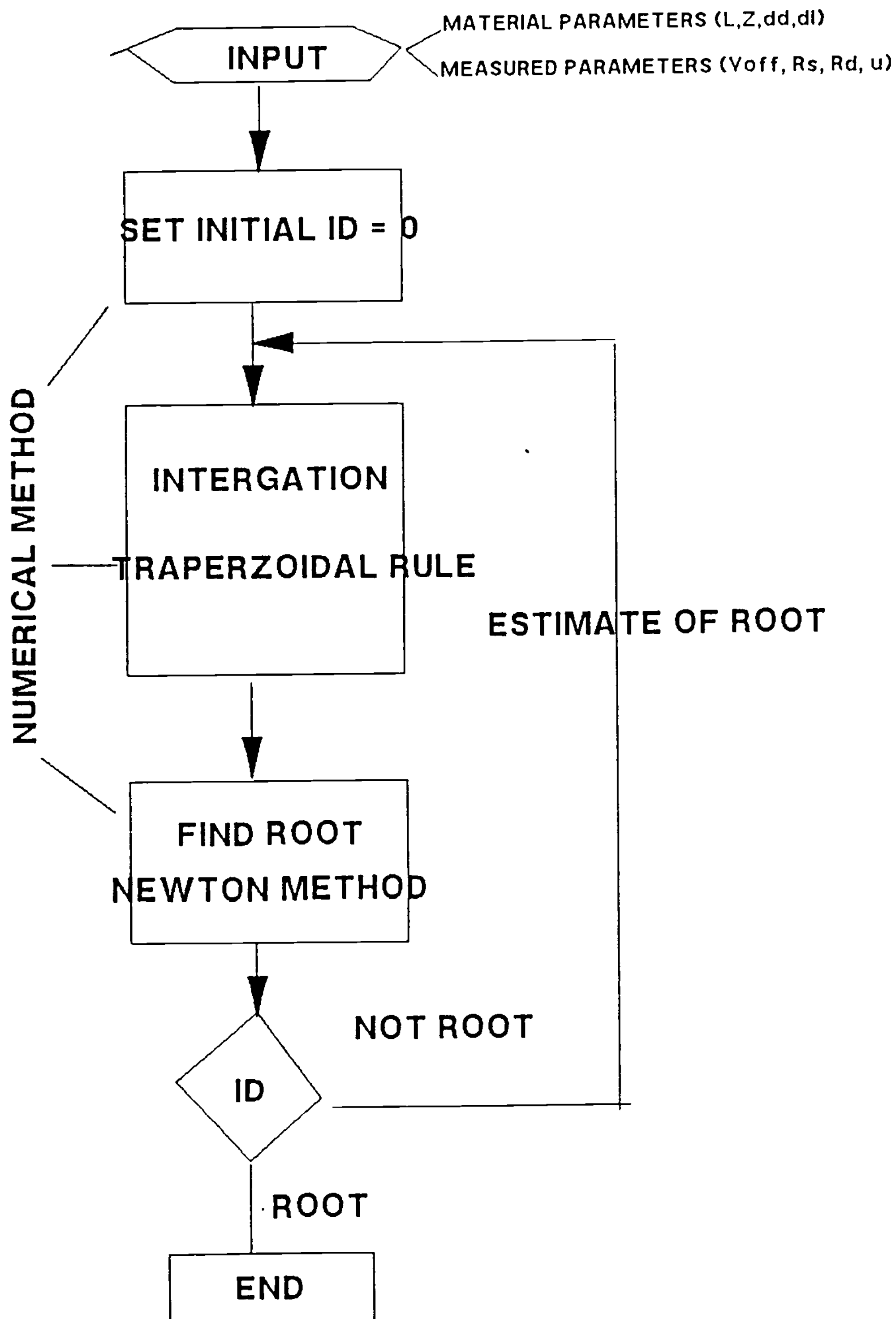

Figure 2.6 Flowchart of I-V curve fitting routine.

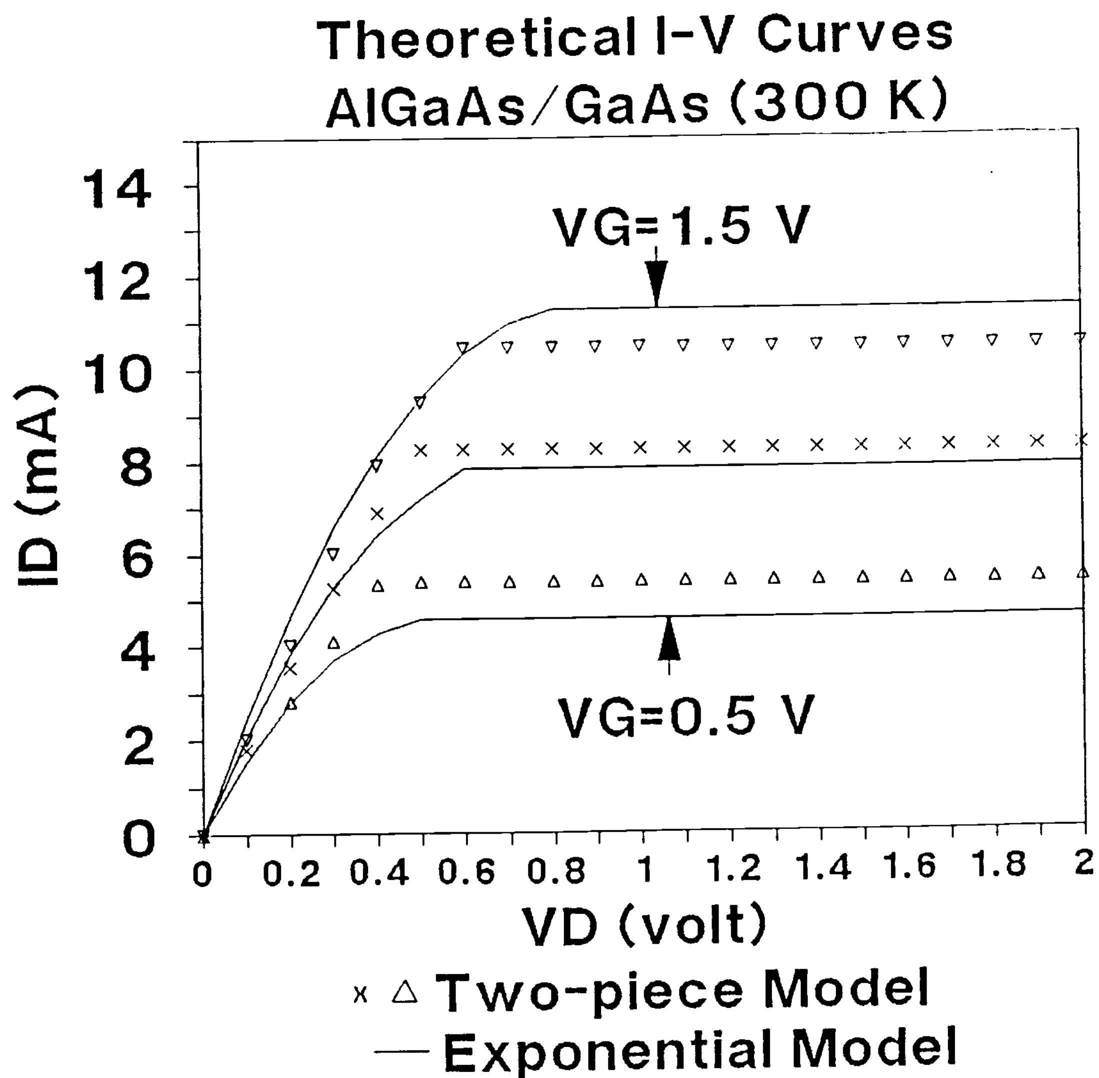

Figure 2.7 Comparison of the I-V Curves for the two-piece model and the exponential model.

3. Experimental

3.1 Material Growth and Device Fabrication

Two different processed wafers, H100 and H108, were obtained from Triquint Inc, in Beaverton, OR. H100 is an AlGaAs/GaAs channel structure as shown in Fig. 3.1. This sample was grown using metal-organic chemical vapor deposition (MOCVD) by the Oregon Graduate Center. The HEMT structure consists of a 3-4 μm undoped GaAs p- type channel followed by a 960 Å $Al_{0.28}Ga_{0.72}As$ layer doped with Si to 1.3 X 10^{18} cm^{-3} and 1070 Å GaAs cap layer doped to the 2 X 10^{18} cm^{-3}. Mesa isolation patterns were defined photolithographically and etched using a wet etch in order to adjust the threshold voltage, V_{off}. Source and drain ohmic contacts were fabricated using e-beam evaporation of Au/Ge/Ni which were subsequently alloyed at 450 C for 1 min. Final metallization was performed using e-beam evaporation of Ti/Pd/Au.

H108 is an pseudomorphic InGaAs channel shown in Fig. 3.2 and grown using molecular beam epitaxy (MBE) by GAIN Electronics Corporation. It primarily includes a 5000 Å undoped GaAs buffer layer, a 100 Å undoped $In_{0.25}Ga_{0.75}As$ channel, a 30 Å spacer layer of undoped $Al_{0.25}Ga_{0.75}As$ and a 200 Å $Al_{0.25}Ga_{0.75}As$ layer doped with Si to 2 X 10^{18} cm^{-3}. The device patterns and metallizations are same as for sample H100. The layers under gate were either wet and dry chemically recessed in order to obtain depletion-mode or

enhancement-mode devices respectively as discussed previously in chapter 2. The devices on sample H108 are all depletion-mode devices.

The six devices on each wafer which were used in my study are different gate length (0.5 μm - 16 μm) structures with 1 μm gate-to-source and gate-to-drain spacing on the each device. The layout (mask specifications) of the six devices are shown in Fig.3-3. Since all the structures and materials on a given wafer were identical except for the gate length, the six devices can be used to study the long channel to short channel scaling behavior of HEMTs. In particular as will be shown later, we have used these devices to characterize the influence of various material parameters, Rs, Rd and the channel mobility on the performance of HEMTs fabricated at Triquint, Inc. Using the saturated velocity as a fit parameter to the I-V curves, we can predict improvements in the performance of HEMTs in the two AlGaAs/GaAs and AlGaAs/InGaAs systems.

3.2 Characterization

The system used to measure the DC characteristics of the devices in the present study is shown in Fig. 3-4. The advantage of using the HP 4145B parameter analyzer are that the device characteristics may be easily programmed and stored on floppy disk for later use in parameter extraction using the numerical models discussed in the last chapter. Measurements were performed primarily at room temperature for a variety of DC characteristics such

as I-V, transconductance, channel conductance and saturation current, the results of which will be discussed in the next chapter.

1070 A (2 E 18) GaAs
960 A (1.3 E 18) AlGaAs x = 0.28
3 - 4 um p- GaAs Buffer

x = Al Mole Fraction

Figure 3.1 Epitaxial layers for H100

Figure 3.2 Layer Structure of H108

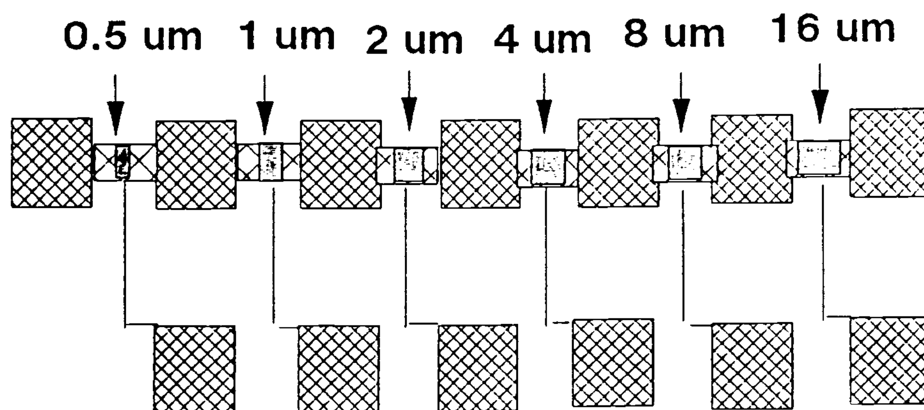

Figure 3.3 Layout of the variable gate length HEMTs in my study.

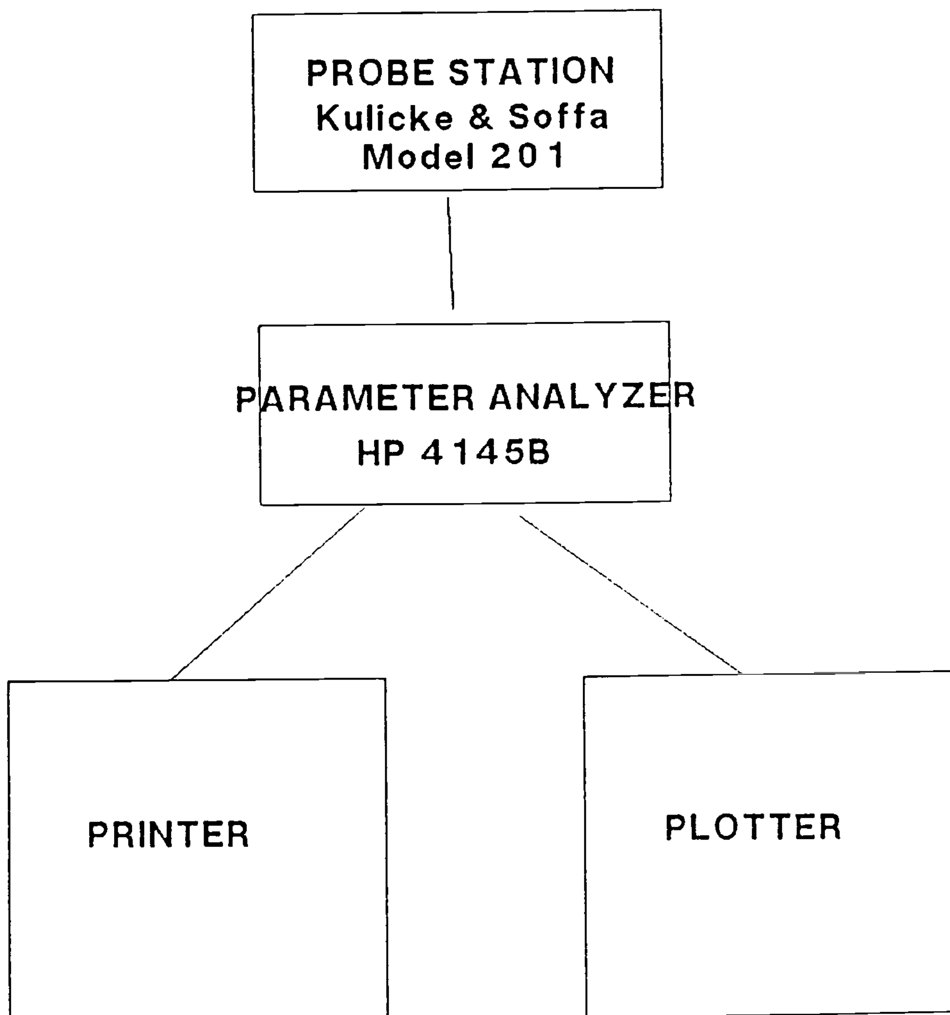

Figure 3.4 Measurement system for DC device characterization

4. RESULTS

4.1 Device Performance

4.1.1 Drain Current

Typical I-V curves for 0.5 μm and 8 μm gate length devices from wafer H100 are shown in Figs. 4-1 and 4.2. Figures 4.3 and 4.4 show I-V characteristics of 0.5 μm and 8 μm gate length devices for the pseudomorphic HEMT sample H108. As is evident from these figures, the drain current increases as the gate length decreases as predicted from the device scaling relations of chapter 2. Comparing with the saturated current equation (2.34) from the two-piece model, when the gate length is reduced the current is higher assuming the gate length dependence of β. As is evident from Figs. 4-1 to 4-4, the saturation current varies approximately linearly with V_G-V_{off}, even for the 8 μm device. This implies that saturation is due to velocity saturation and not pinchoff. However, another important effect is the parasitic MESFET effect discussed later when the doped AlGaAs layer is no longer depleted. This effect also causes nonideal behavior for large gate biases.

In addition to the above samples, another sample, H110 (the AlGaAs/GaAs system) was fabricated by Triquint Inc. with the same structure as the sample H108 (the AlGaAs/InGaAs system) and fabricated at the same time. The device performance of H110 was far

inferior to the that of devices from H108, which seems to suggest that the DC performance of the InGaAs pseudomorphic HEMTs are superior to that of the GaAs channel HEMTs.

4.1.2 Transconductance

Typical transconductance characteristics versus applied gate voltage (V_{GS}) at a fixed drain voltage V_{DS} Of 2.5 V are shown in Fig. 4.5 for sample H100 and Fig. 4.6 for sample H108. From these figures, the maximum transconductance of H100 is 130 ms/mm and for H108 is 155 ms/mm which occur for the shortest gate length devices. The increase of the transconductance with gate length is apparent from the 2-piece model, equation (2.37), as long as the channel is sufficiently long. In the limit of short channel devices, equation (2.35) predicts no increase with decreasing gate length.

The peak in the transconductance versus gate voltage curves occurs when the parasitic MESFET in the AlGaAs is turned on. The parasitic MESFET is formed by the gate and doped AlGaAs layer when gate voltage larger than[31]

$$V_t = V_{off} + (V_{po})_{2D} \tag{4.1}$$

where

$$(V_{po})_{2D} = q n_{so} (d + \Delta d)/\varepsilon \tag{4.2}$$

is the pinchoff voltage of the 2DEG and n_{so} is the maximum equilibrium 2DEG concentration calculated in section 2.3. From the equation (4.2), we obtain $(V_{po})_{2D}$ = 0.93 V for the H100 and 0.73 V for H108, respectively. Comparing to the measured

transconductance characteristics (Figs. 4.5 and 4.6), the parasitic MESFET effect is apparent at the gate voltages close to the theoretical values. Since the 1D models presented in chapter 2 did not include the parasitic MESFET effect, we fit the I-V curves only in the regime of sufficiently low gate bias such that no parasitic effects occur.

4.1.3 Saturation Current

The saturation current characteristics for various applied gate voltage at a fixed drain voltage of 2.5 V are shown in Fig. 4.7 for H100 and Fig. 4.8 for H108. Comparing the theoretical saturated current equation (2.34) from the two-piece model to Figs. 4.7 and 4.8, when the gate length is reduced the current is higher due to the gate length dependence of β. The saturation current is an important quantity to determine the saturated drift velocity in the present study. By fitting the saturation current versus L for different gate biases, an estimate for υ_S is made in the regime where no parasitic MESFET effects occur. Hence, we can estimate the saturated velocity using the DC results from the HP parameter analyzer without the need of other measurements.

4.2 Device Characteristics

In order to compare the 1D exponential model with the experimental I-V characteristics, the physical parameters V_{off} (the

threshold voltage), Rs (the source resistance) , Rd (the drain resistance), and μ (the mobility) must be know. In this section, we use the DC device characteristics in order to determine the parameters V_{off}, Rs, Rd, and μ at room temperature. These parameters are used later in fitting the I-V characteristics using the 1D models discussed previously in chapter 2.

4.2.1 Threshold Voltage and Mobility

In order to ascertain the threshold voltage and channel mobility, we use the conductance versus gate voltage at small drain voltages. The total resistance of the the channel under small drain bias is composed of the channel resistance and the source and drain series resistances

$$R_{total} = L/[\mu C(V_G - V_{off})W] + R_{s+d} \qquad (4.3)$$

where R_{s+d} is the total series resistance in device, V_{off} is the threshold voltage, μ is the channel mobility, W is the gate width, and

$$C = \varepsilon_2/(d + \Delta d) \qquad (4.4)$$

is the effective gate capacitance per unit area. From the (4.3), we obtain the total conductance

$$g_D = g_{s+d}\frac{C_{2D}(W/L)\mu(V_G-V_{off})}{C_{2D}(W/L)\mu(V_G-V_{off})+g_{s+d}} \qquad (4.5)$$

where g_{s+d} is the total series conductance. From equation (4.5) and Fig. 4.9 of G_D vs. V_G , we can determine the threshold voltage when the channel conductance is equal to zero. The measurement threshold voltages of the devices in my study are shown in table 4.1.

From the equation (2.24), the threshold voltage depends on the Schottky barrier height, Φ_b, the conduction band discontinuity and the doped AlGaAs thickness. From experimental measurement of the Au-Schottky barrier height variation versus Al mole fraction in doped $Al_xGa_{1-x}As$ layer,[32] the Schottky barrier heights here are estimated to be 1.2 V for H100 (x = 0.28) and 1.16 V for H108 (x = 0.25). The conduction band discontinuity is estimated as 0.23 V for H100 (for the $Al_{0.28}Ga_{0.72}As/GaAs$ interface assuming 67% of the bandgap difference occurs in the conduction band[16]) and 0.44 V for H108 (for the $Al_{0.25}Ga_{0.75}As/In_{0.25}Ga_{0.75}As$ interface[17] assuming 65% of the bandgap difference occurs in the conduction band), although there still exists significant discrepancy in the experimentally measured values. The effective thickness of doped AlGaAs layer, d_d, can be determined from the threshold voltage assuming the ionized donor concentration is known using equation (2.24). The results for d_d are shown in the Table 4.2. The threshold voltages for H100 show some variations due to the apparent difference in thickness of the doped AlGaAs layer under the gate. The doped AlGaAs thickness shows some variation because the process of recess gate etching is somewhat difficult to control, and thus there may exist nonuniformities in the thickness. Nouniformities may be also exist for the Schottky barrier height Φ_b due to processing.

Differentiating equation (4.3) with respect to gate length at the same V_G-V_{off} gives

$$dR_{total}/dL = 1/[\mu C(V_G - V_{off})W] \qquad (4.6)$$

where R_{s+d} is the total series resistance in the device, V_{off} is the threshold voltage, μ is the mobility and W is the gate width. Hence, the mobility can be obtained from the slope of curve of R_{total} vs. L. From the Figs. 4.10 and 4.11, we obtain an average mobility of 3397 cm^2/V sec for sample H100 and 3995 cm^2/V sec for sample H108.

4.2.2 Source and Drain Series Resistance

The technique for determining Rs and Rd is based on the "end" resistance measurement[33]. The schematic of the "end" resistance measurement is shown in Fig 4.12. In this figure, the gate-source current results in a voltage drop across the source series resistance Rs with the drain contact floating as a probe. Hence, the floating drain potential, V_{DS}/I_{GS}, is

$$V_{DS}/I_{GS} \cong (Rs + 0.5\ R_{ch}) \tag{4.7}$$

where the channel resistance, R_{ch}, is equal to r_{ch} L/W with r_{ch} the distributed channel resistance. The results are shown in Figs. 4.13 and 4.14 for H100 and H108, respectively. From Figs. 4-13 and 4-14, Rs and Rd can be obtained when Rch is equal to zero, that is, L=0. By extrapolating the curves in 4.13 and 4.14, we find Rs ≅ Rd ≅ 38 Ω for sample H100 and Rs ≅ 45 Ω, Rd ≅ 73 Ω for sample H108. The reason for the different value of Rs and Rd in sample H108 may be due to mask misalignment. Compared to the best state of the art devices, thesis series resistances are somewhat high and thus limit the performance of the present devices.

4.3 Model Fits Using the Exponential Model

In chapter 2, the exponential 1D model was introduced as a better approximation than the two piece model to the velocity-field characteristics. In this section, we use the exponential 1D model with the experimental data Rs, Rd, μ and V_{off} to fit the saturation current using υ_s, the saturated velocity, as the only fit parameter. Figures 4.15 and 4.16 show the saturation current vs. the gate length at several different gate biases for device from H100 and H108, respectively. The values of the saturated drift velocity which result in the best qualitative fit to the data are found to be 8 x 10^6 cm/sec for H100 and 1.1 x 10^7 cm/sec for H108. For the AlGaAs/GaAs device, the value of the saturated drift velocity of the sample H100 is the same as value measured for GaAs/AlGaAs device by Masselink et al.[9] For the pseudomorphic HEMT, H108, the saturated drift velocity is somewhat lower than the value 1.3 x $10^{\cdot 7}$ cm/sec predicted from equation (1.1). In fitting the I-V characteristics using the saturated velocity, the sensitivity of the fit to the value of saturated velocity is close to 40 % if υ_s is varied from 1 x 10^7 cm/sec to 2 x 10^7 cm/sec, which gives some indication of the error involved.

The comparison of the experimental and theoretical I-V curves of 0.5 μm and 8 μm for H100 are shown in Figs. 4.17 and 4.18 and for H108 are shown in Figs 4.19 and 4.20. Figures 4.17 through 4.20 shows fairly good agreement between the theoretical and experimental current voltage data, with a noticeable discrepancy in

the fit for the shortest gate length devices due to finite channel conductance effects in the saturation regime.

L (gate length)	V_{off}	
	H100	H108
0,5 um	-2.1 V	-1.5 V
1 um	-1.9 V	-1.55 V
2 um	-1.5 V	-1.45 V
4 um	-1.85 V	-1.4 V
8 um	-2.1 V	-1.4 V
16 um	- 2.0 V	-1.35 V

Table 4.1 The threshold voltages for samples H100 and H108.

L (gate length)	d_d	
	H100	H108
0,5 µm	575 A	390 A
1 µm	550 A	395 A
2 µm	510 A	385 A
4 µm	545 A	380 A
8 µm	560 A	380 A
16 µm	565 A	375 A

Table 4.2 The thickness of the doped AlGaAs layer for samples H100 and H108 calculated from the threshold voltage data, Table 4.1.

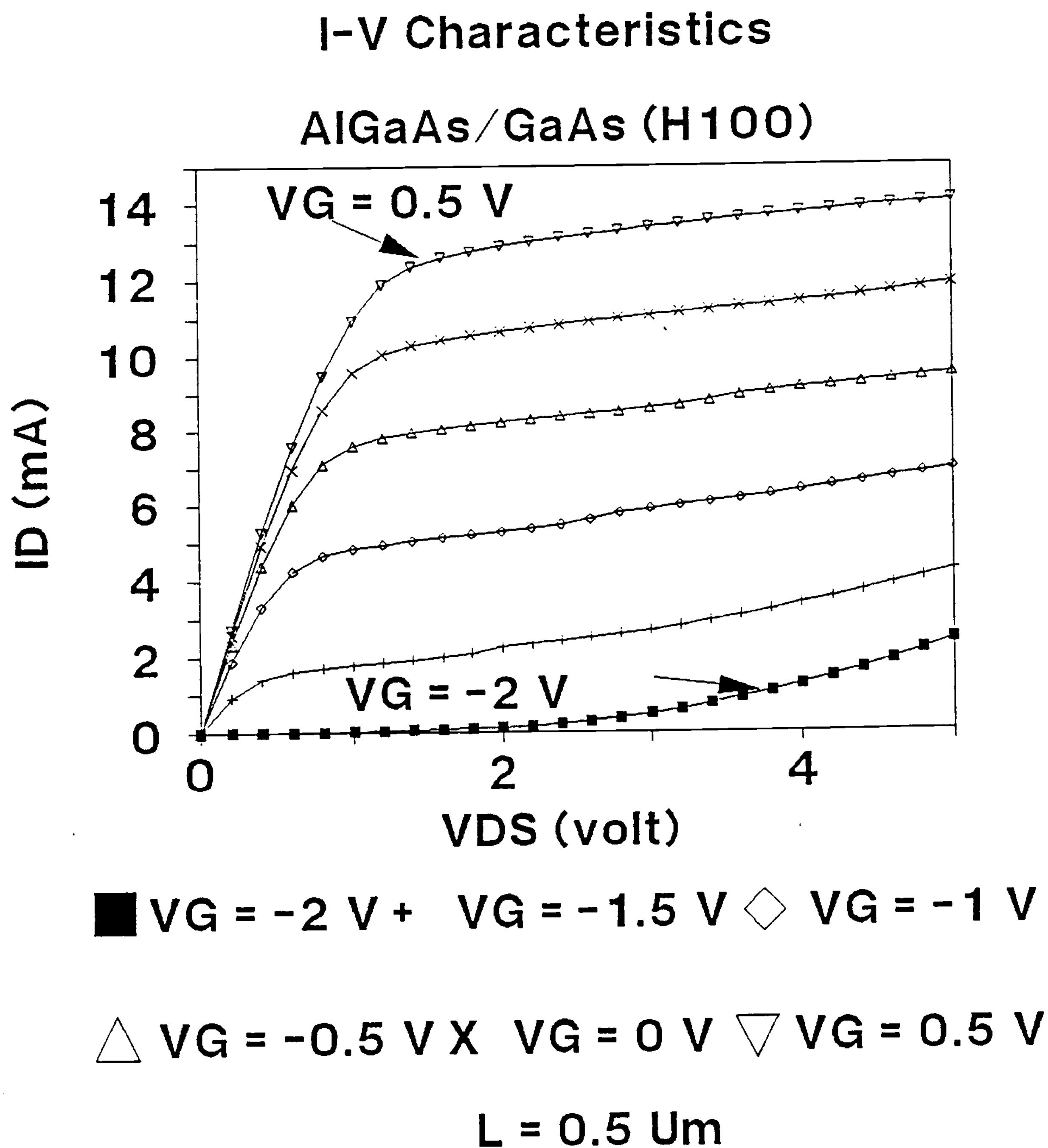

Figure 4.1 I-V curves of H100 (L = 0.5 um).

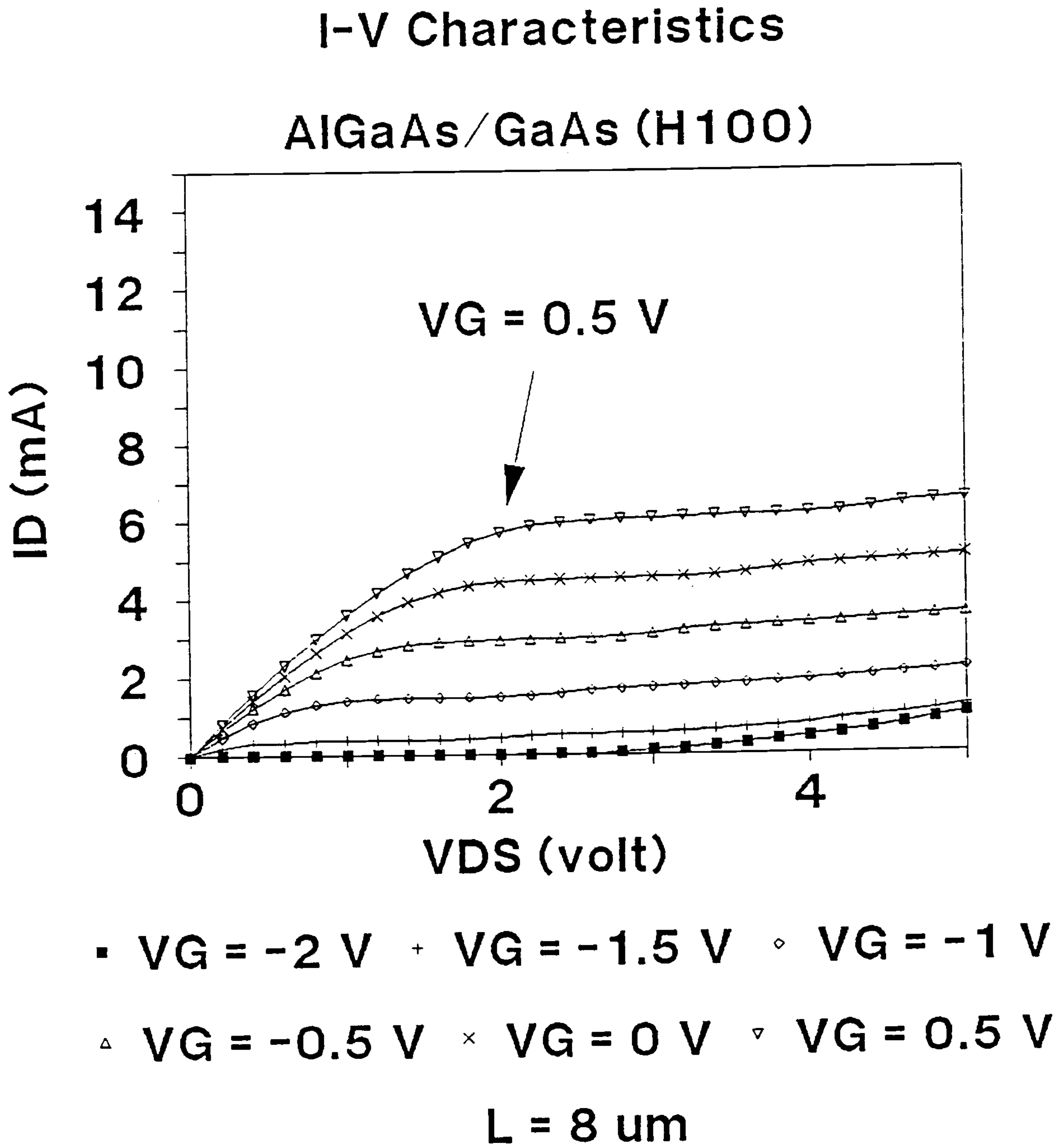

Figure 4.2 I-V curves of H100 (L = 8 um).

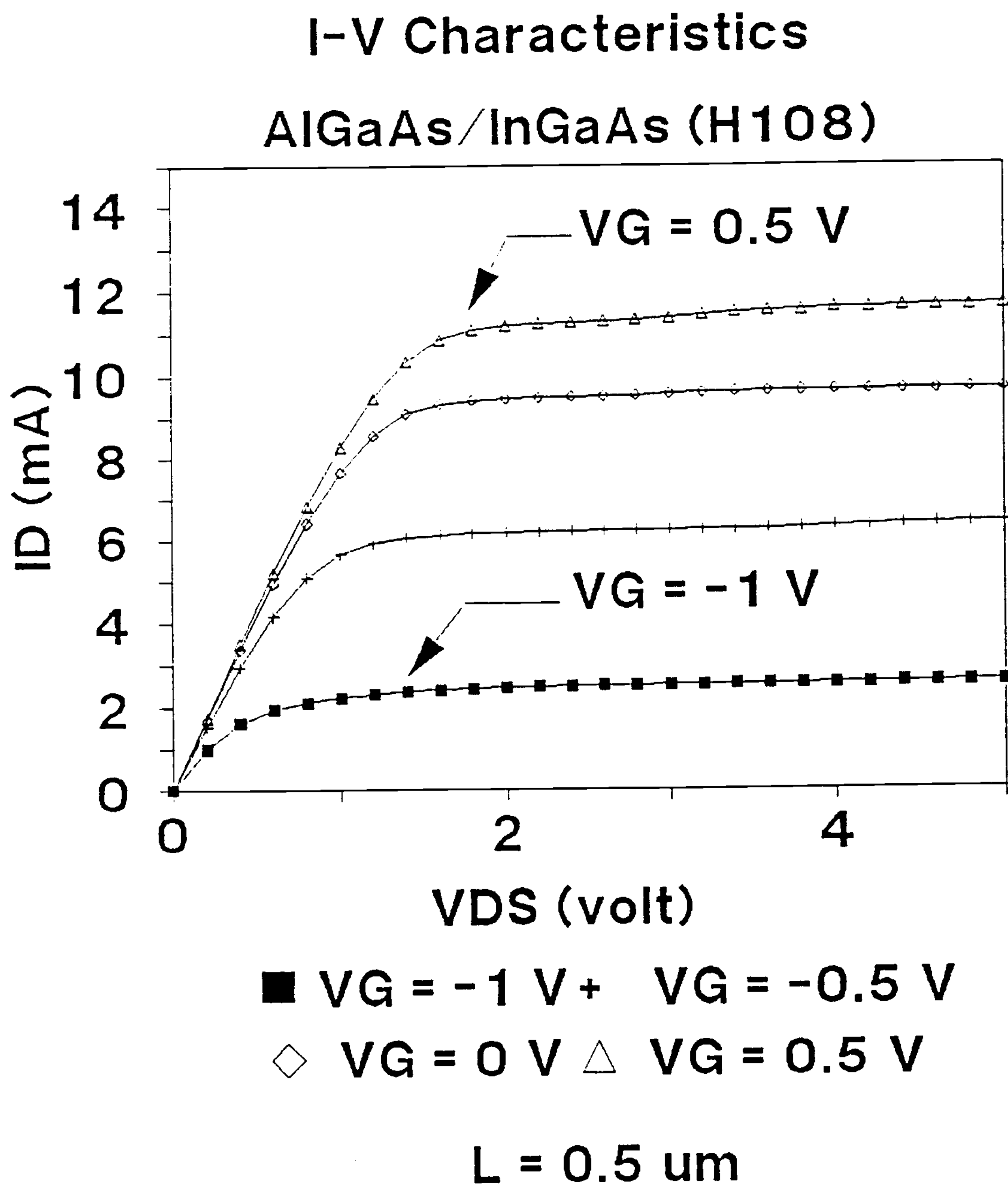

Figure 4.3 I-V curve of H108 (L = 0.5 um)

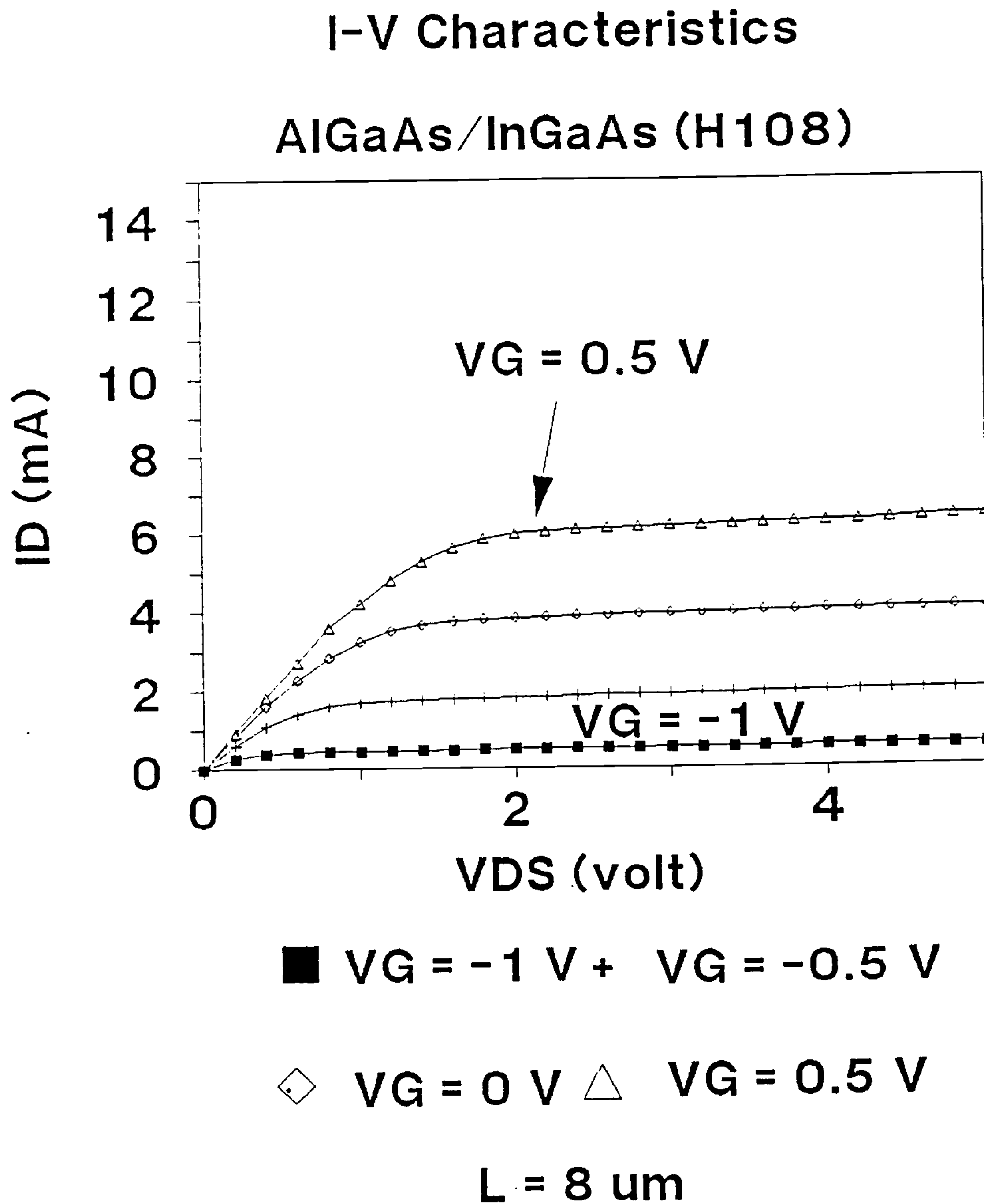

Figure 4.4 I-V curve of H108 (L = 8 um)

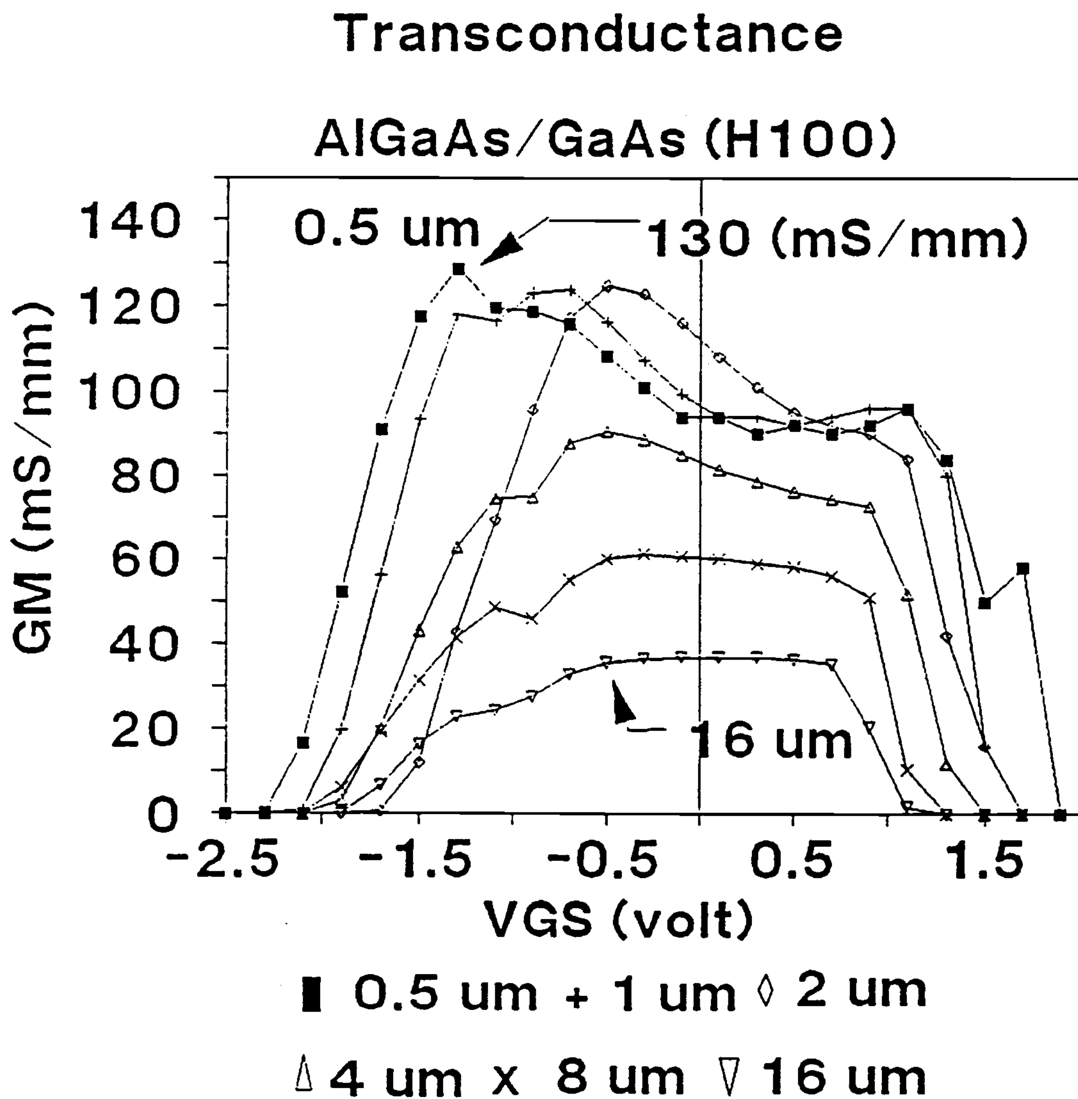

Figure 4.5 Transconductance at function of gate voltage for H100.

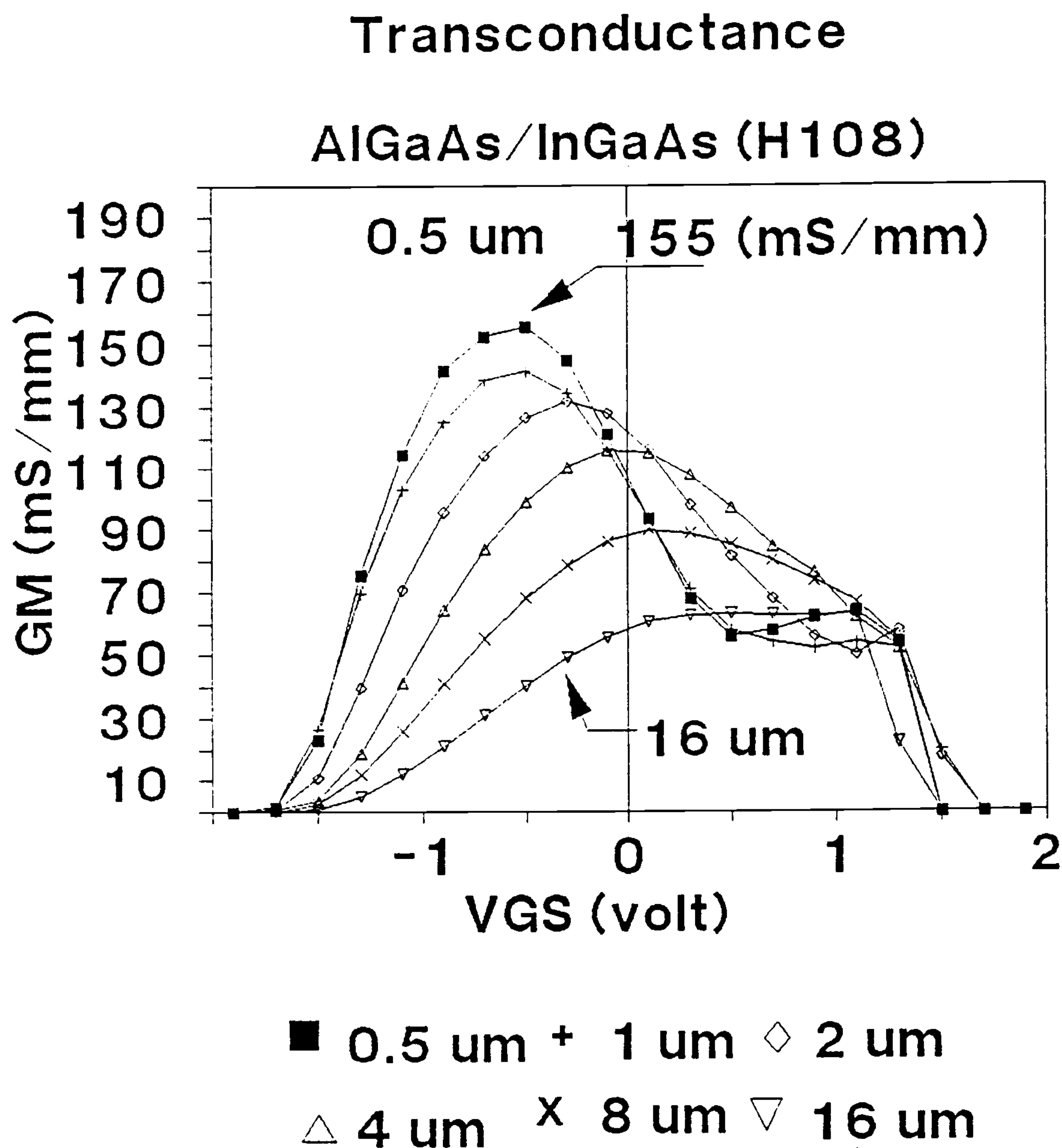

Figure 4.6 Transconductance at function of gate voltage for H108

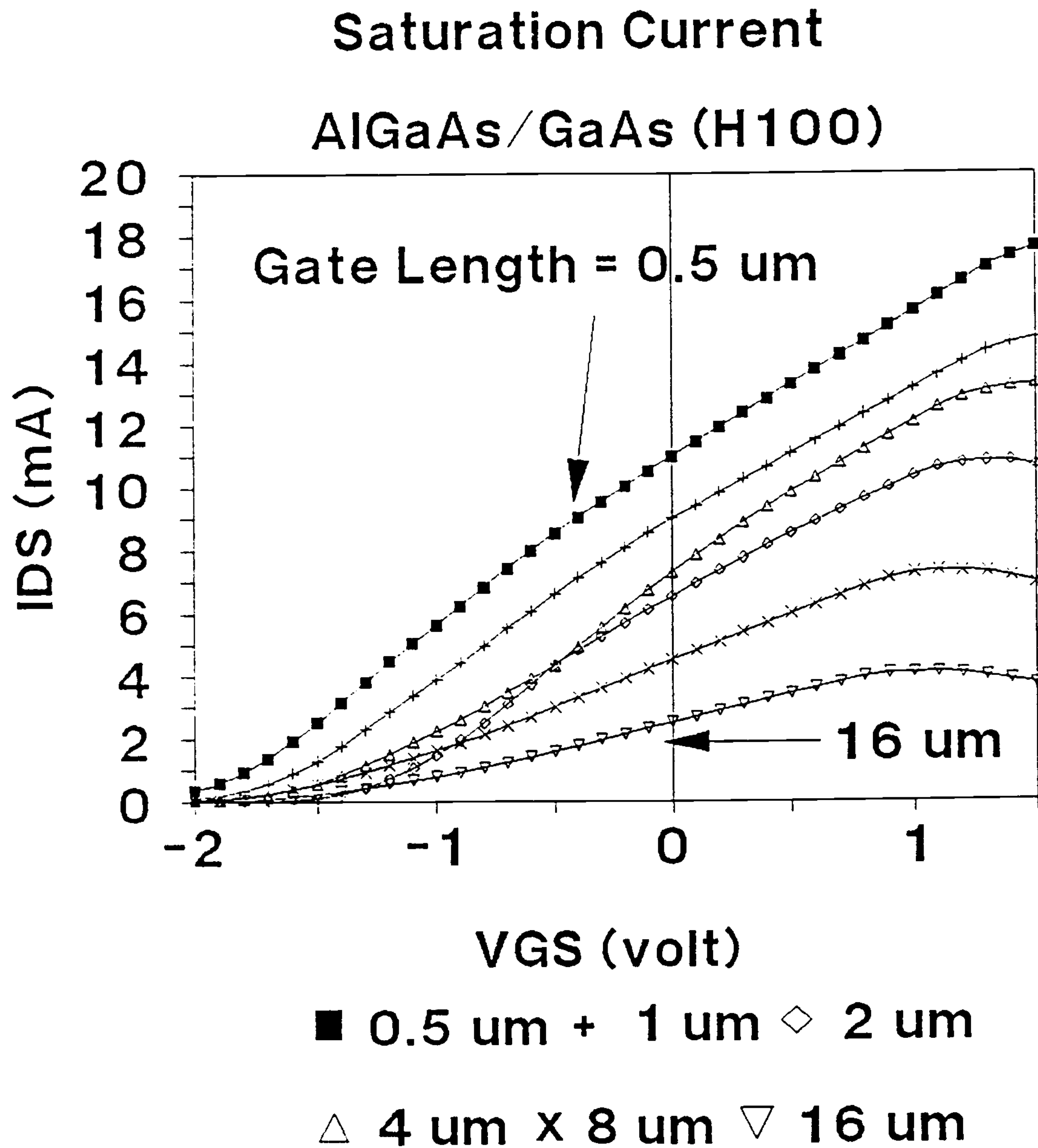

Figure 4.7 Saturation current at function of gate voltage for H100

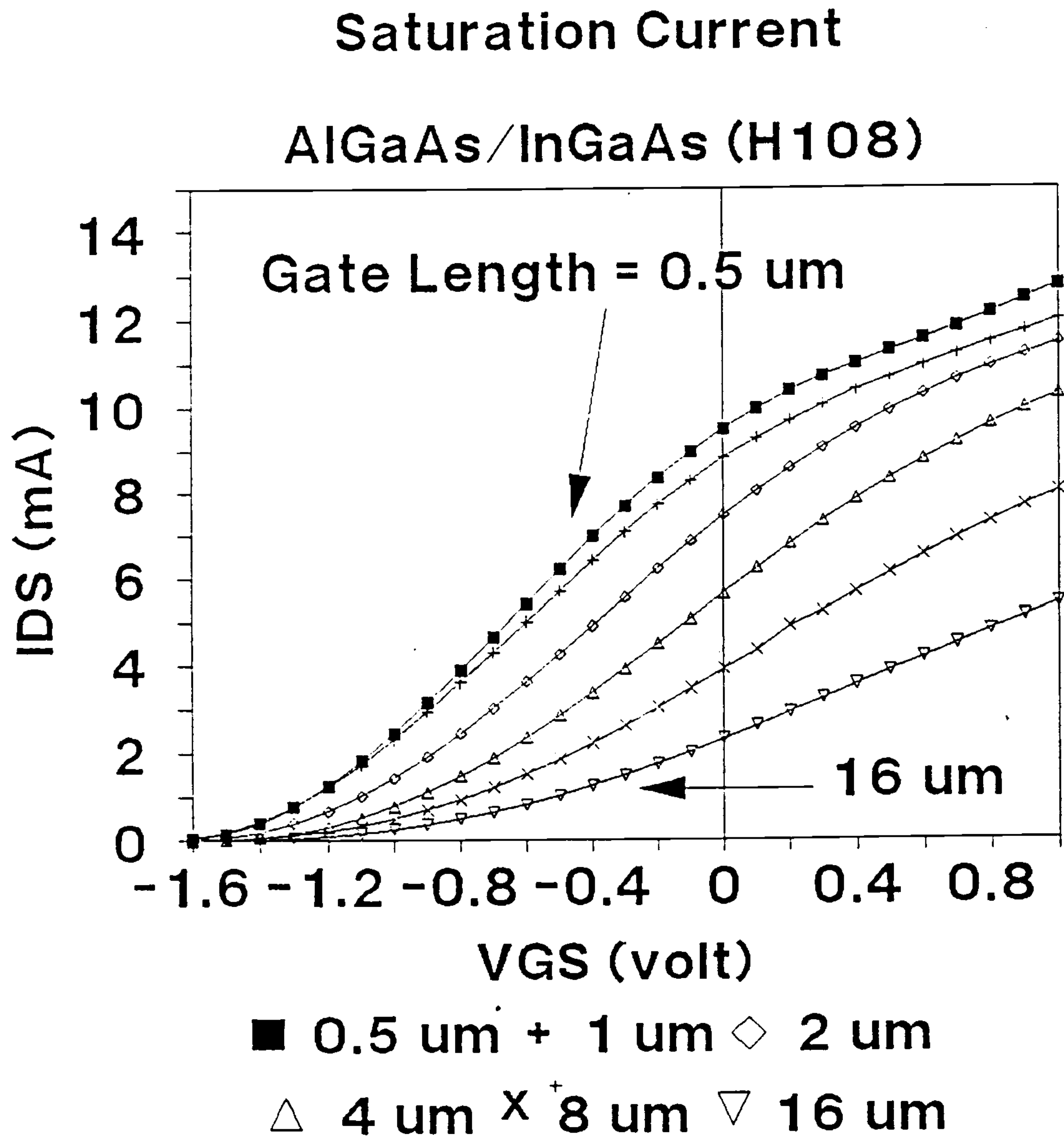

Figure 4.8 Saturation current at function of gate voltage for H108

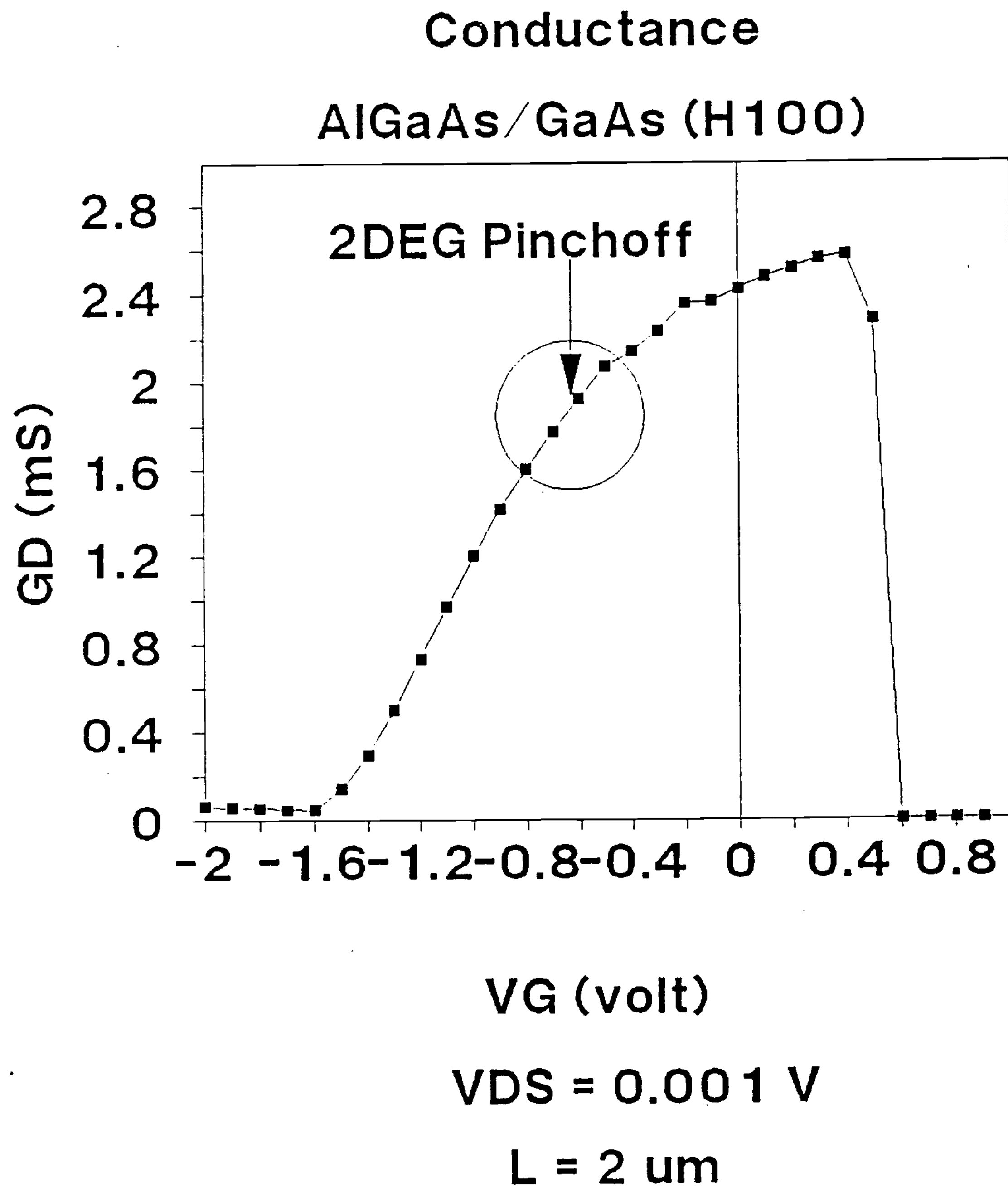

Figure 4.9 Conductance at function of gate voltage (H100, L = 2um)

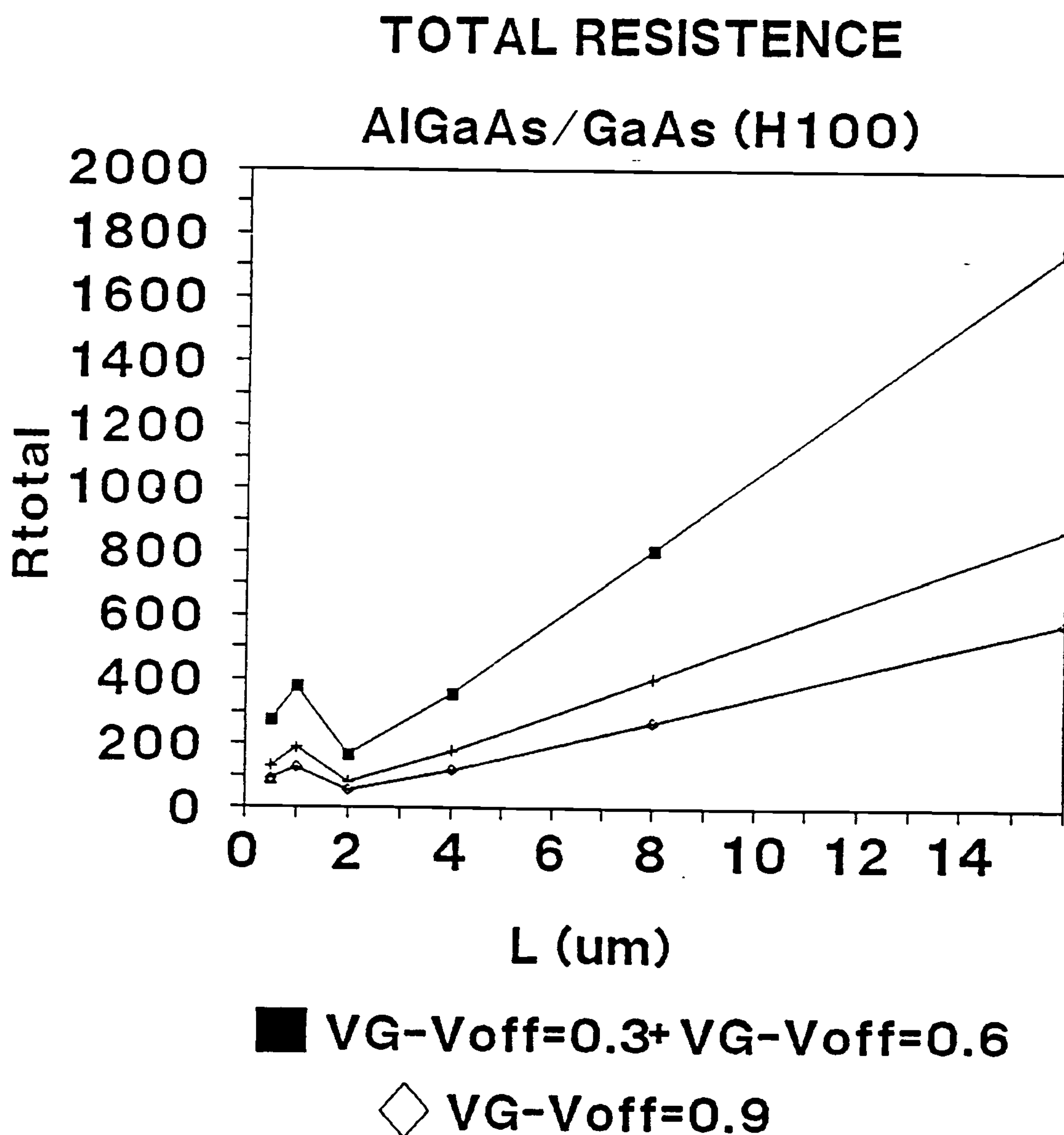

Figure 4.10 Total resistance of the H100.

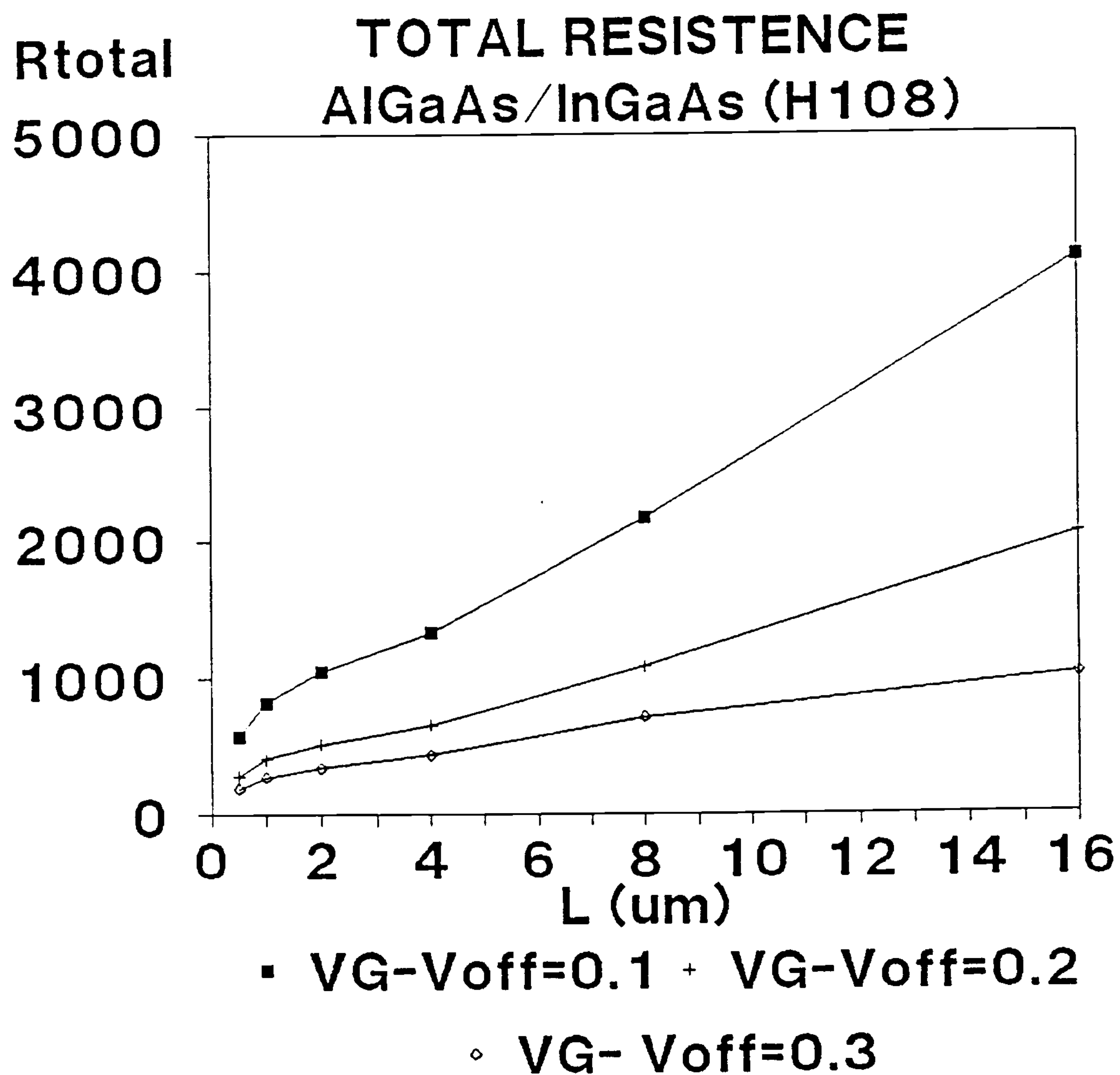

Figure 4.11 Total resistance of the H108.

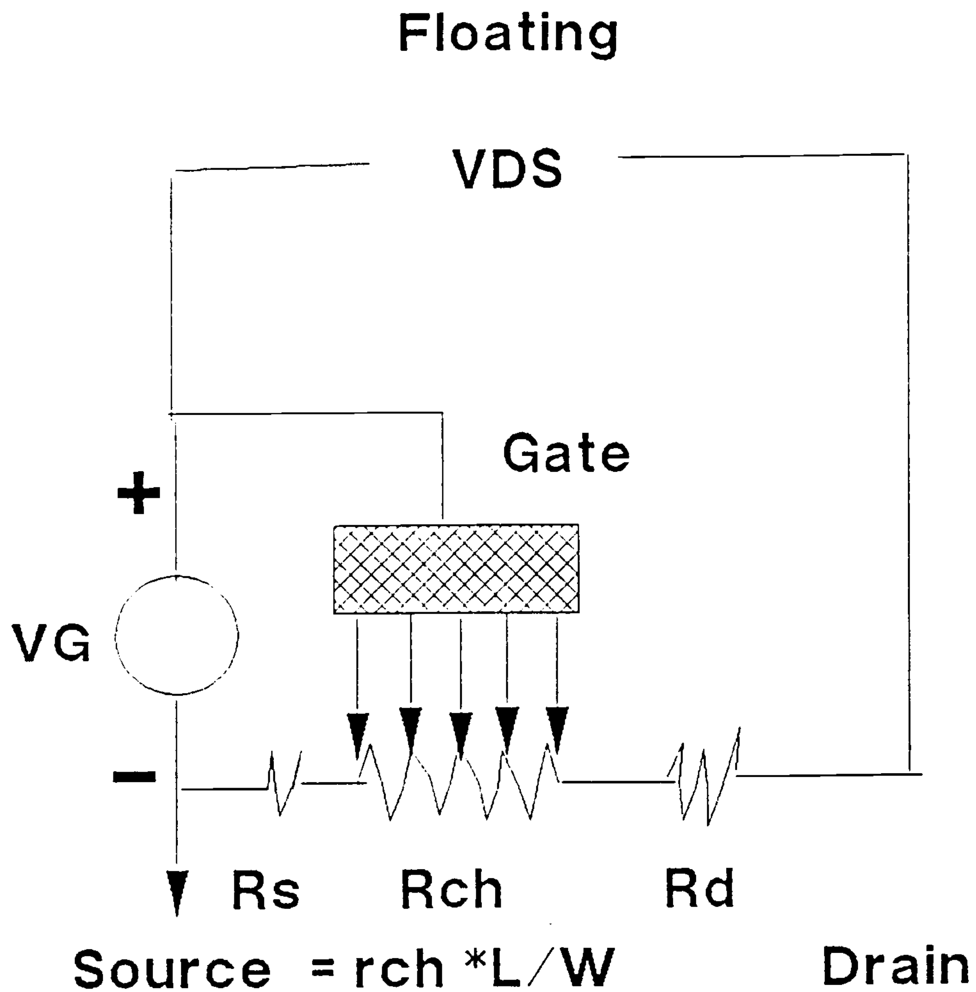

Figure 4.12 "end" resistance measure technique

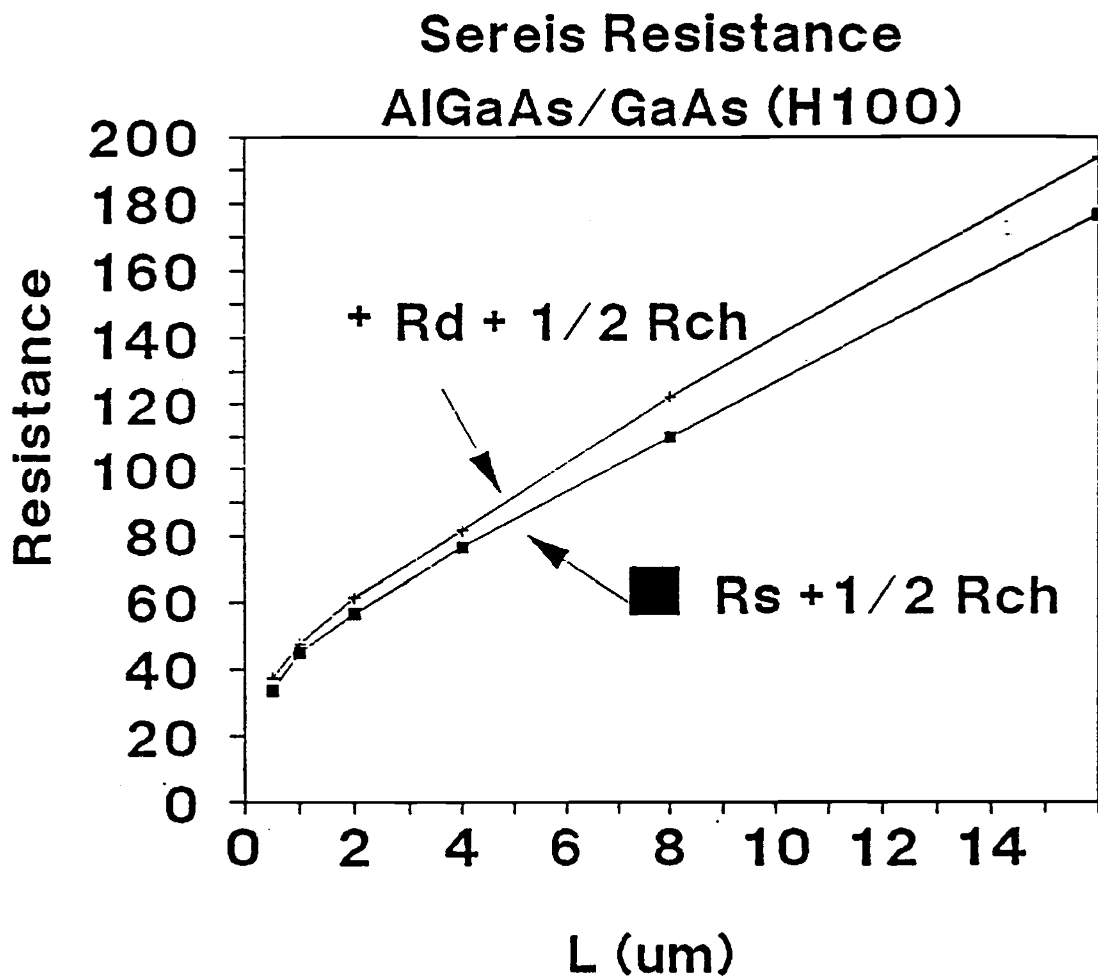

Figure 4.13 "end" resistance measurement for the H100.

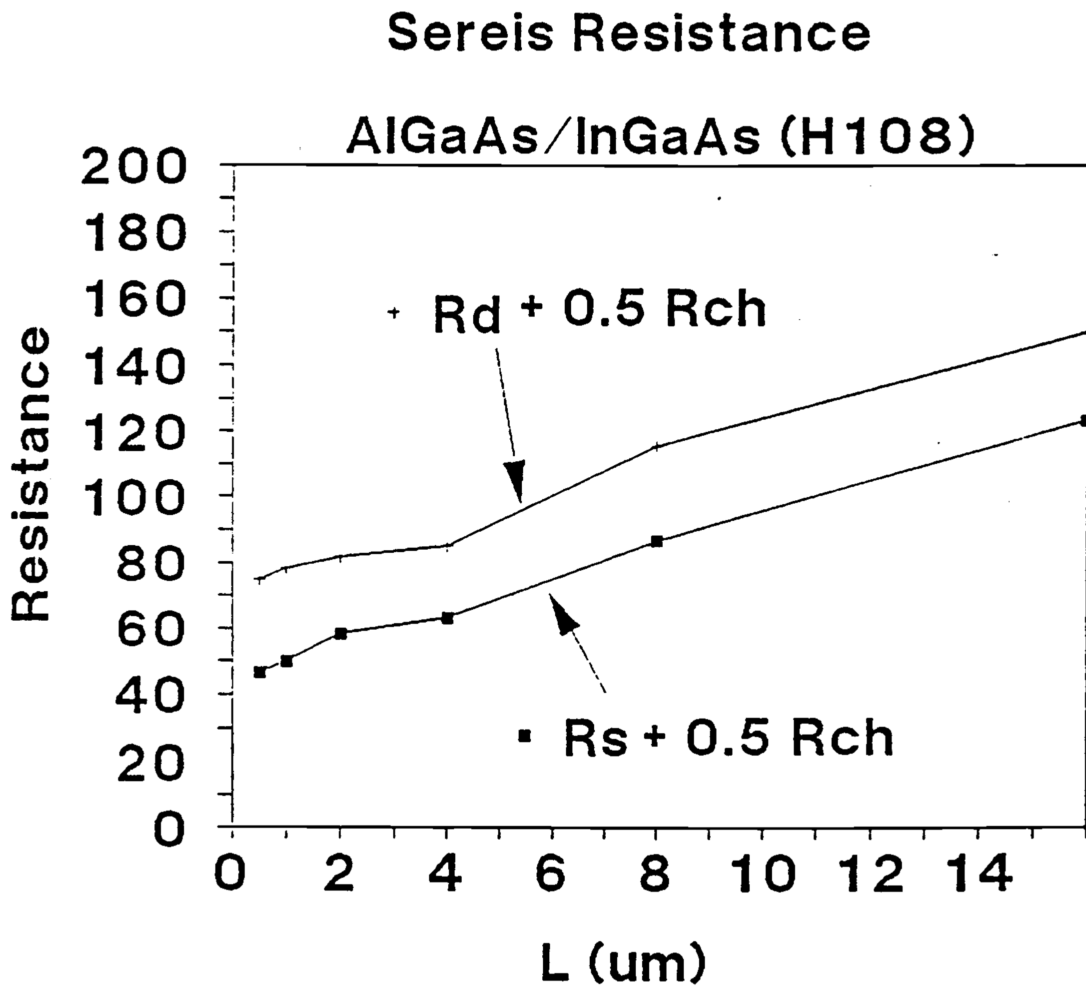

Figure 4.14 "end" resistance measurement for the H108.

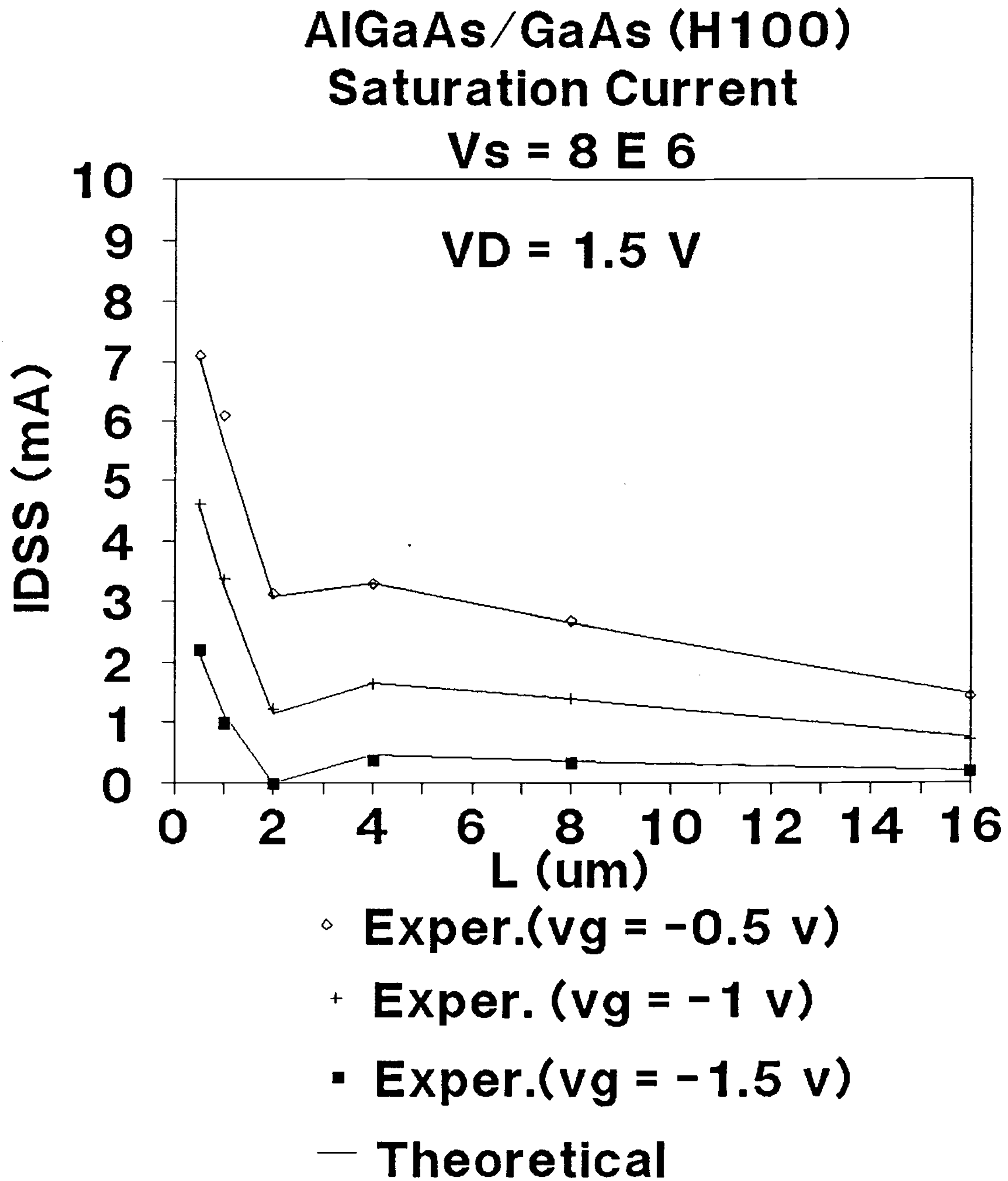

Figure 4.15 Saturation current vs. gate length at different gate bias for H100.

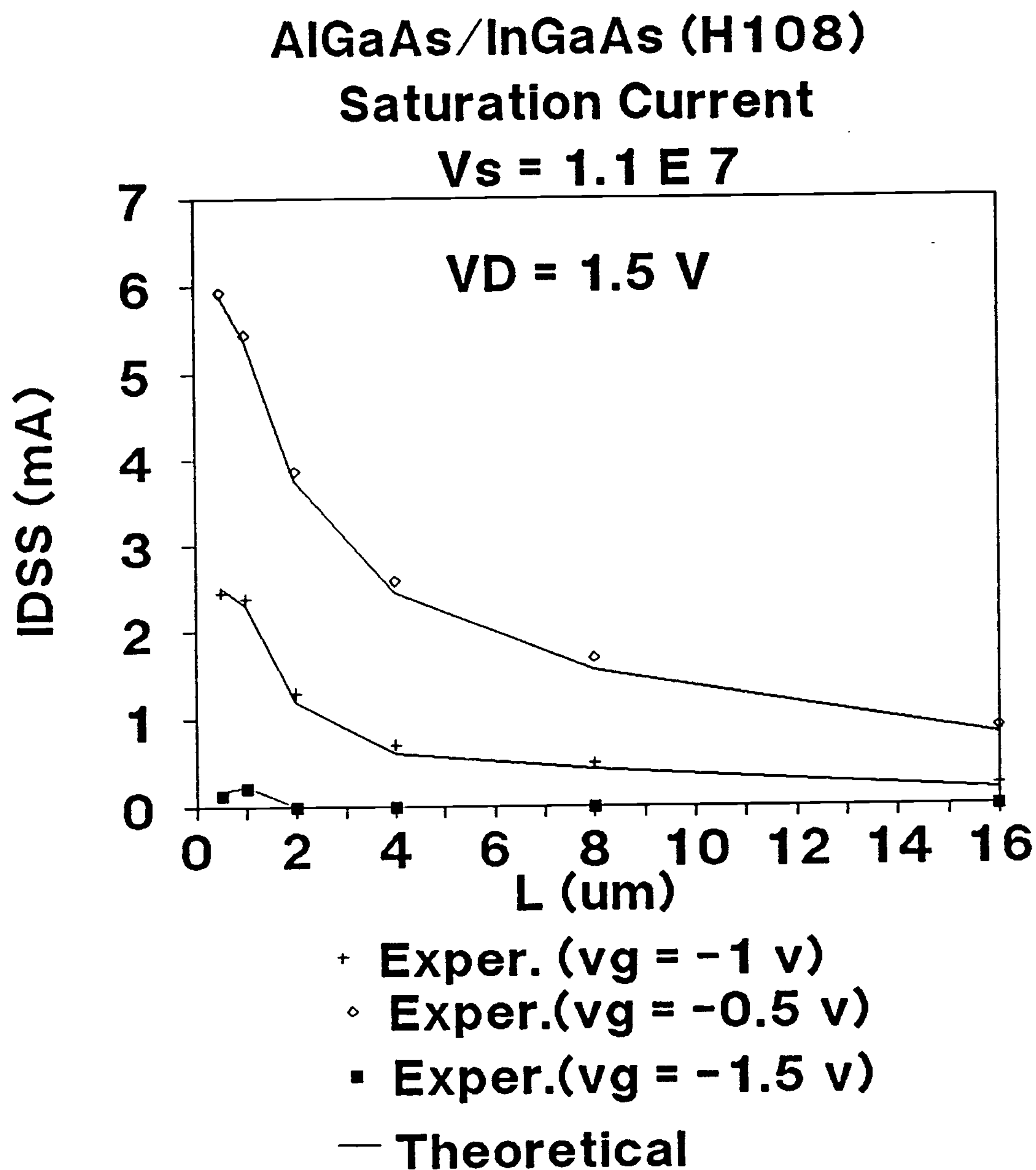

Figure 4.16 Saturation current vs. gate length at different different gate bias for H108.

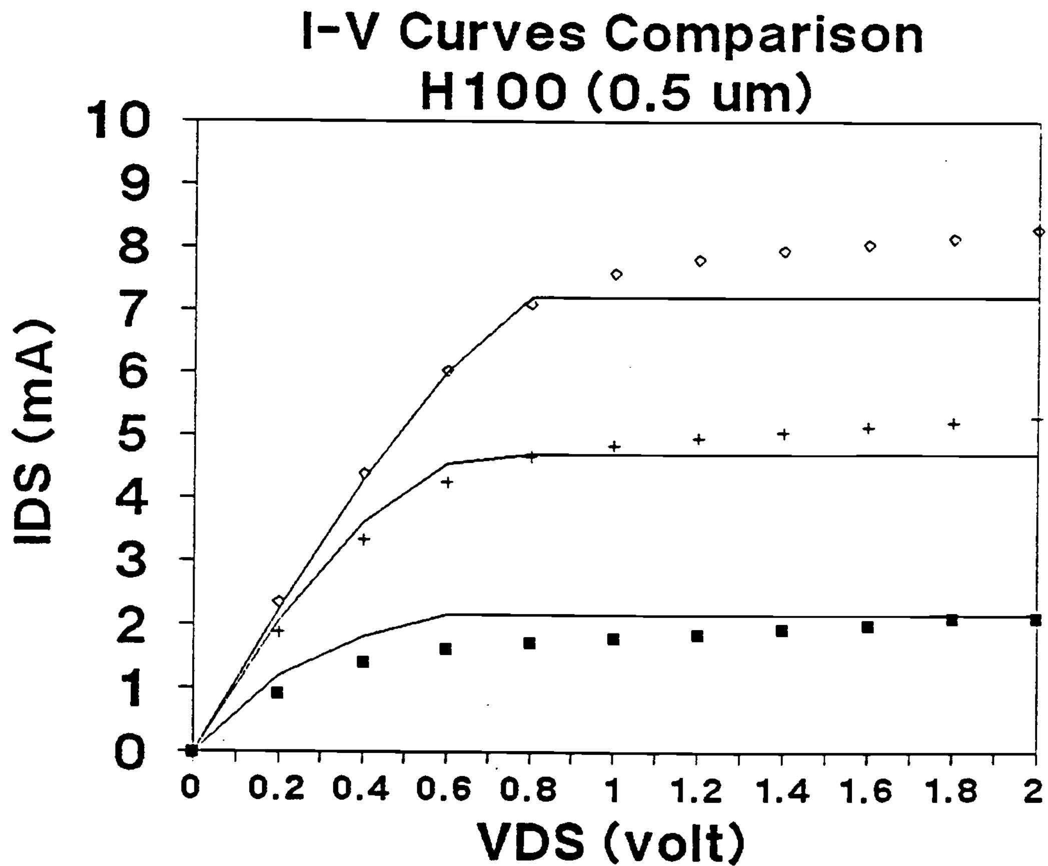

Figure 4.17 Theoretical and experimental I-V curves for H100 (L = 0.5 μm).

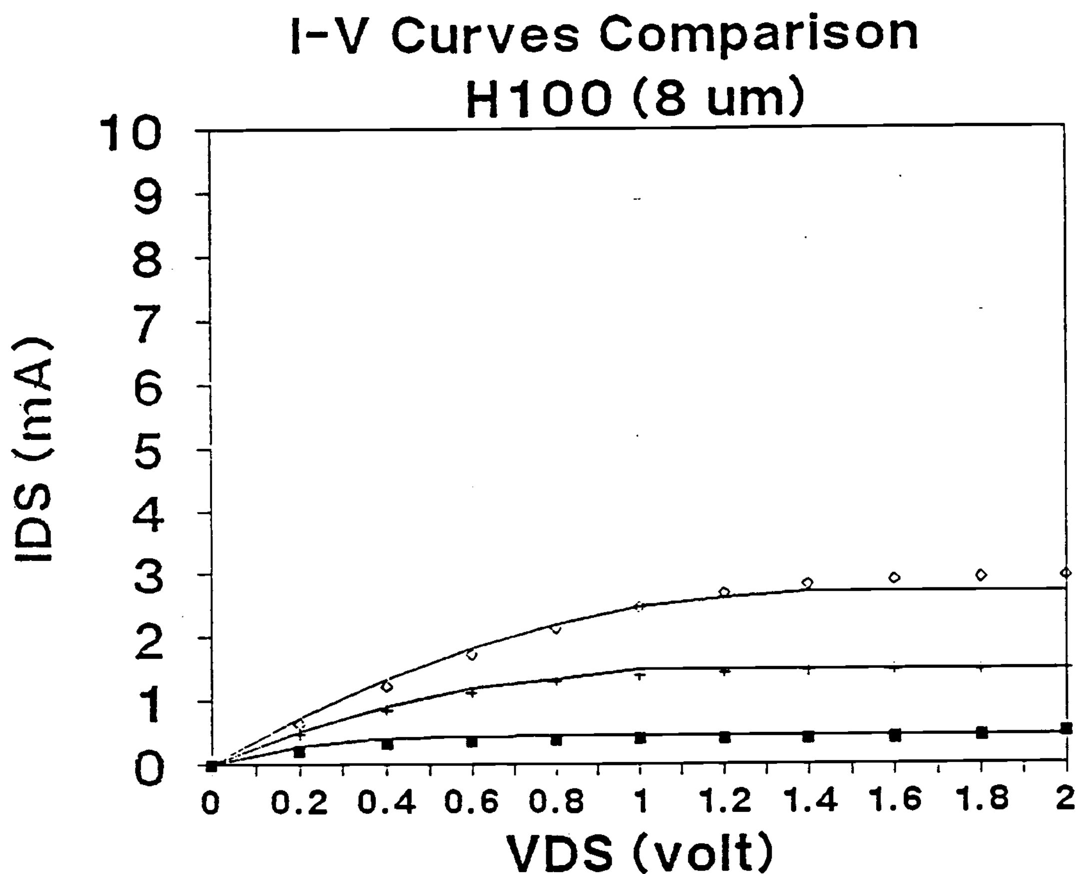

Figure 4.18 Theoretical and experimental I-V curves for H100 (L = 8 μm).

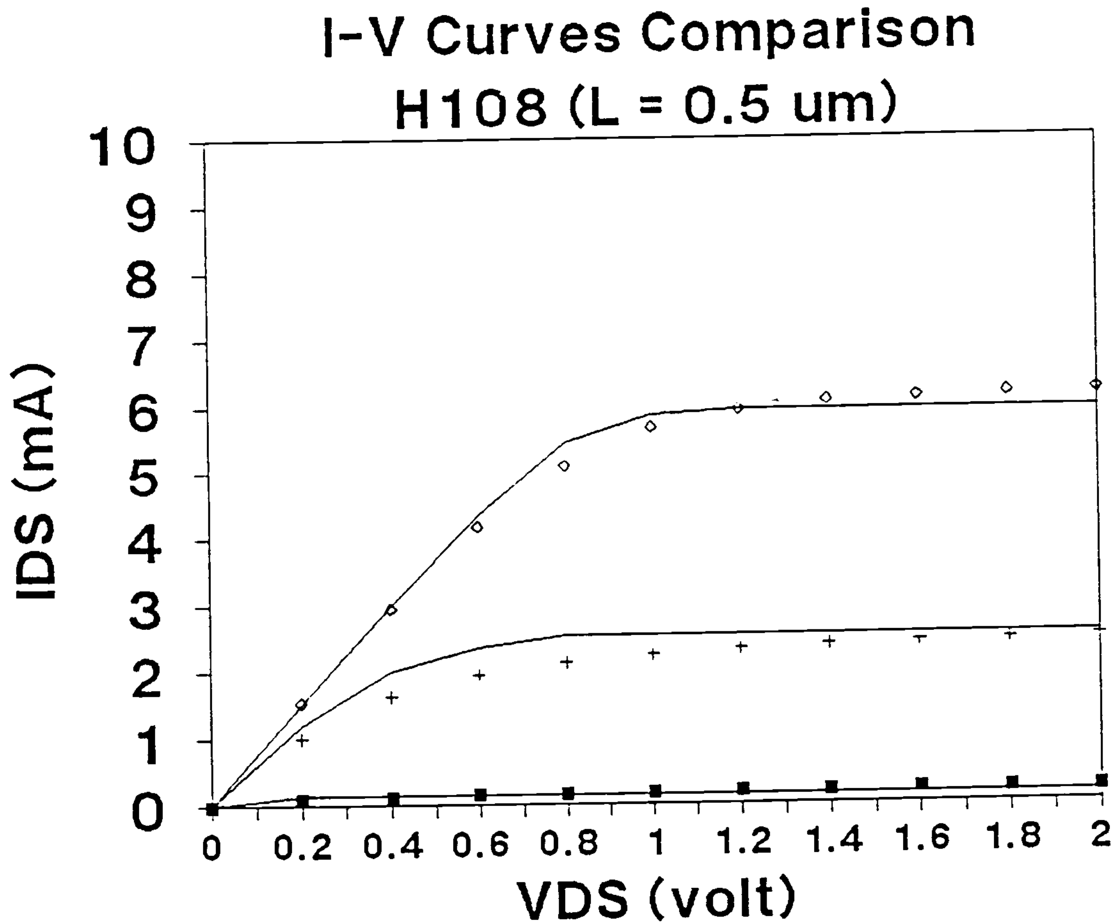

Figure 4.19 Theoretical and experimental I-V curves for H108 (L = 0.5 um).

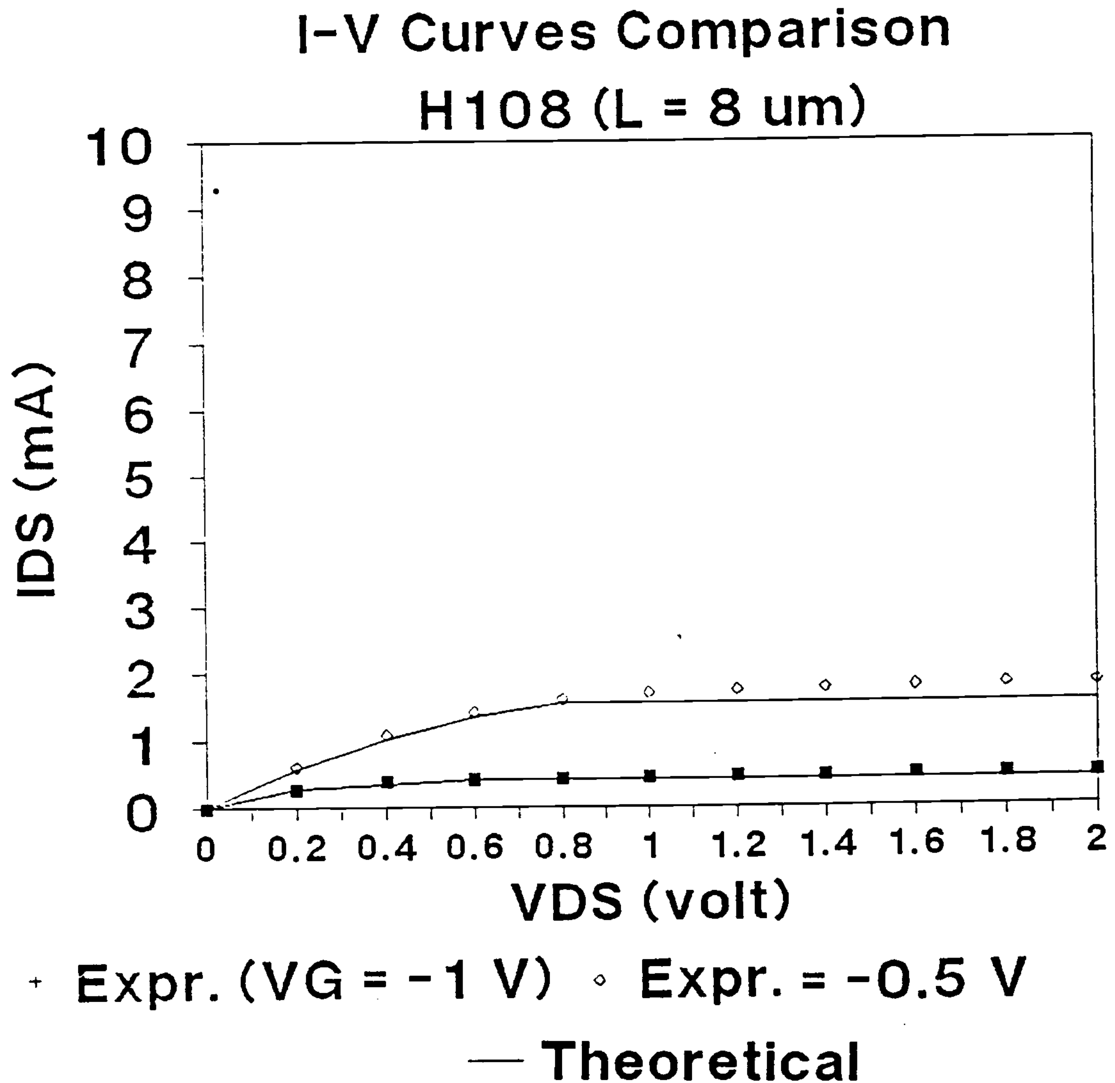

Figure 4.20 Theoretical and experimental I-V curves for H108 (L = 8 um)

5. DISCUSSION OF RESULTS

The model parameters which were derived from the DC characteristics in the present study are Rs (the source resistance), Rd (the drain resistance), μ (the mobility), υ_s (the saturation velocity), and V_{off} (the threshold voltage). These parameters are summarized in table 5.1 for both systems.

The drain series resistance may be divided between the drain ohmic contact resistance and gate-to-drain spacing channel resistance. In the region between the gate and drain (or source), the doped AlGaAs layer is ungated and has a relatively large thickness compared to the gate region which is recess etched to control the threshold voltage. The 2DEG concentration in these regions corresponds to the equilibrium concentration, n_{so}, given by equation (2.17). These regions contribute an effective series resistance to the channel which may be approximated as

$$R = L/(n_{so}\, q\, \mu Z) \qquad (5.1)$$

where L is the channel length between the gate and the drain or source, Z is the channel width and μ the mobility. From equation (5.1), the contribution to Rs and Rd due to the channel region may be calculated for the 1 µm gate-to-source and gate-to-drain spacing on each device, respectively. For sample H100, the calculated Rd is 32 Ω which is close to the measured value of 38 Ω from table 5.1. This

result seems to indicate that the gate-to-drain channel resistance is the dominant contribution to the total series resistance, which may be decreaseing the source-to-gate and drain-to-gate spacing.

Compared to the bulk mobility of GaAs which is 8500 cm^2/V at 300K, and the the bulk mobility of InAs which is 33000 cm^2/V, the measured values of mobility 3397 cm^2/V sec for H100 and 3995 cm^2/V sec for H108, respectively, are not very high. Part of the reason for the low mobility on sample H100 may be associated with the fact that no spacer layer was grown between the GaAs/AlGaAs interface to reduce ionized impurity scattering. The reason for the low mobility on sample H108 may be due to alloy scattering in the InGaAs channel, although this is usually significant only at lower temperatures. Hence, the high series resistance (Rs and Rd) and low mobility limits the performance of the present devices. If one could decrease Rs and Rd to 5 Ω by reducing the gate-to-source and gate-to-drain spacing and increase the mobility to 6800 cm^2/V sec for sample H100, we increase the current to 70% as shown in the Fig. 5.1 for a 8 μm. For a 0.5 μm device, one cannot easily predict how much improvement in device performance can be expected due to short channel effects for this gate length device.

The results of fitting the saturated drift velocity gave 8×10^6 cm/sec for sample H100 and 1.1×10^7 cm/sec for sample H108. The saturated drift velocity of sample H100 is the same as the value of measured by Masselink[9]. The saturated drift velocity for sample H108 is somewhat lower than the value 1.3×10^7 cm/sec calculated using equation (1.1). Equation 1.1 is a simple linear interpolation, and does

not include many second order effects which may enter into the actual saturated drift velocity. Therefore the value obtained here is reasonable.

Figures 4.17 through 4.20 show fairly good agreement between the 1D exponential model and experimental current voltage data. Thus, the 1D exponential model is good compared to the discontinuous two-piece model, and can be included into SPICE models to simulate HEMTs circuits. However, the present 1D model is not sufficiently accurate to account for short channel effects such as the slope of the saturation current with drain bias, which would require additional model parameters.

In order to improve the understanding the HEMT device characteristics, future works with the present devices should include:

a) Independent evaluation of mobility using Hall effect measurements.

b) Measure the DC and transient device characteristics at cryogenic temperature in order to study DX center effect (persistent photoconductivity and I-V collapse), as well as the device performance at low temperature.

c) Perform frequency dependent measurements to characterize the small signal characteristics and parameters.

d) Improve the HEMTs device model to include more realistic models for the velocity overshoot in the GaAs velocity-field characteristics.

parameters	samples (AlGaAs/GaAs) H100	(AlGaAs/InGaAs) H108
Rs	38 Ω	38 Ω
Rd	45 Ω	73 Ω
υ_S	8.0 E 6 cm/sec	1.1 E 7 cm/sec
μ	3400 cm2/Vsec	3995 cm2/Vsec

Table 5.1 The measurement physical parameters for samples H100 and H108.

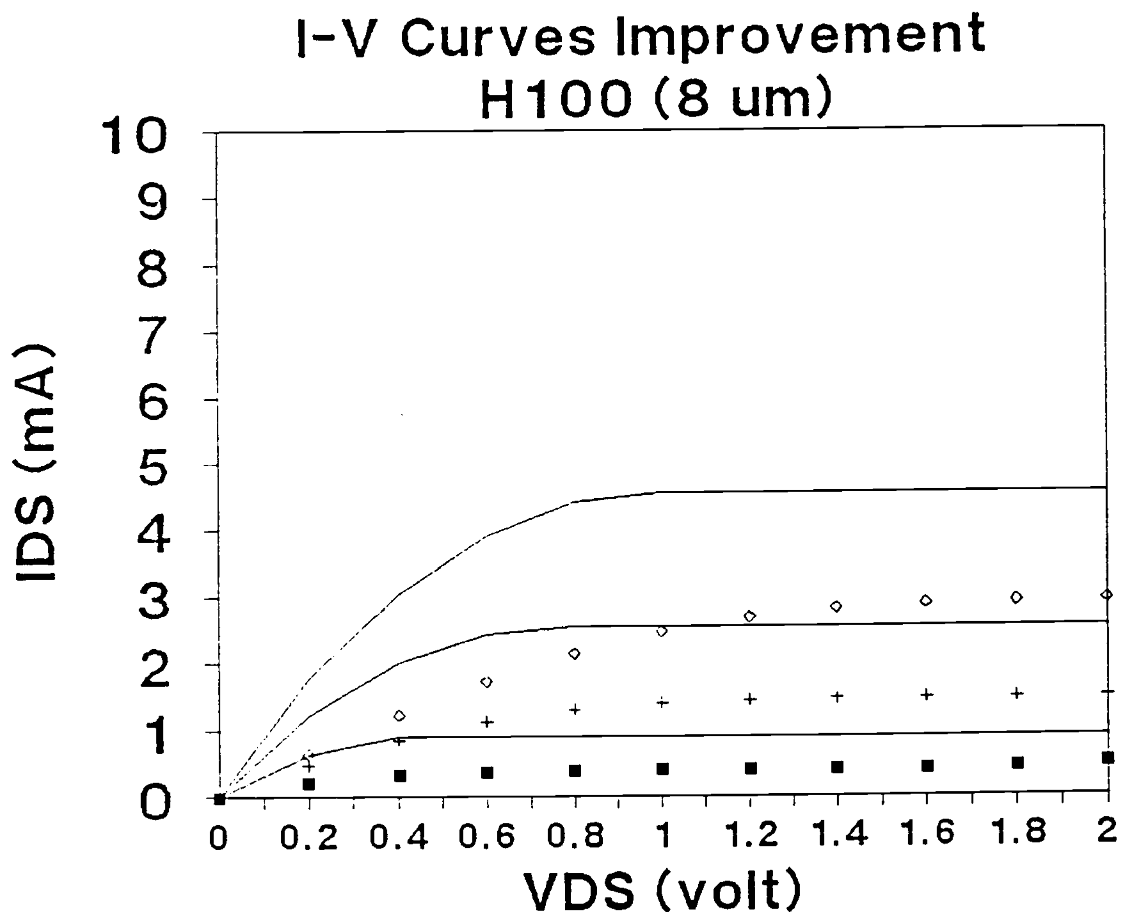

Figure 5.1 Improvement in assuming optimized values for Rs, Rd, μ at 300 K I-V curves for H100 (L = 8 um).

BIBLIOGRAPHY

[1] R. Dingle, H. L. Störmer, A. C. Gossard, and W. Wiegmann, Appl. Phys. Lett., vol. 33, p. 665 (1978).

[2] R.A. Anderson, IBM J. Res. Dev. 4, p. 283 (1960).

[3] L. Esaki and R. Tsu, Internal Report RC2418, IBM Research, March 26, 1969.

[4] T. Mimura, S. Hiyamizu, T. Fujii and K. Nanbu, Jpn. J. Appl. Phys., vol. 19, p. L225 (1980).

[5] R. Dingle, M. D. Feuer, and C. W. Tu, "Selectively doped heterostructure transistors:material, devices and circuits", Chapter 6 in VLSI Electronicss, Microstructure Science, vol. 11, Einspruch and Wisseman, Academic Press, New York, 1985.

[6] H. L. Störmer, R. Dingle, A. C. Gossard, W. Wiegmann and M. D. Struge, Sol. St. Comm., vol. 29, p. 705 (1979).

[7] J. Klem, T, J, Drummond, R. Fischer, T. Henderson, and H. Morkoc, Journal of Electronics Materials 13, p. 741 (1984).

[8] D. V. Lang, R. A. Logan, and M. Jaros, Physical Review B 19, p. 1015 (1979).

[9] T. J. Drummond, R. J. Fischer, W. F. Kop, H. Morkoc, K. Lee, and M. S. Shur, IEEE Transaction on electron devices ED-30, p. 1806 (1983).

[10] A. J. Valois, G. Y. Robinson, K. Lee, and M. S. Shur, Journal of Vaccum science Technology B 1, p. 190 (1983).

[11] J. H. van der Merwe, J. Appl. Phys., vol. 34, no. 1, p. 123, Jan. (1963).

[12] A. A. Ketterson, W. T. Masselink, J. S. Gedymin, J. Klem, C.-K. Peng, W. F. Jopp, H. Morkoc and K. R. Glaeson, IEEE Trans. Elec. Dev., vol. ED-33, p. 564 (1986).

[13] S.-M. J. Liu, M. B. Das, C. K. Peng, J. Klem, T. S. Henderson, W. F. Kopp and H. Morkoc, IEEE Trans. Elec. Dev., Vol. ED-33, p. 576 (1986).

[14] W. T. Masselink, W. Kopp, T. Henderson and H. Morkoc, IEEE Elec. Dev. Lett. EDL-6, p. 539 (1985).

[15] W.-P. Hong and P. K. Bhattacharya, IEEE Trans. Electron Dev., vol. ED-34, no. 7, p. 8 (1987).

[16] T. K. Kuech, D. J. Wolford, R. Potemski, J. A. Bradley, K. H. Kelleher, D. Yan, J. Paul Farrell, P. M. S. Lesser, and F. H. Pollak Appl. Phys. Lett. 51(7), 17 p. 505 (1987).

[17] T. G. Anderson, Z. G. Chen, V.D. Kulakovskii, A. Uddin and J. T. Vallin, Solid State Commun. 64, p. 379 (1987).

[18] J. Yashida, IEEE Trans. Elec. Dev., vol.ED-33, p. 154 (1986).

[19] H.L. stormer, R. dingle, A. C. Gossard, W. Wiegmann, and R. A. Logan, Conf. Ser.-- Inst. Phys. 43, p. 557 (1979).

[20] F. Stern, CRC critical Reviews in Solid State Science, 499, May (1974).

[21] L. D. Landau and E. M. Lifshitz, Quantum Mechanics (Non - Relativistic Theory) Oxford: Pergaman Press, p. 74 (1977).

[22] Delagebeaudeuf D. and Linh N. T., IEEE Trans. Electrons Devices, vol. ED-29, p. 955 (1982)

[23] K. Lee, M. S. Shur, T. J. Drummond and H. Horkoc, J. Appl. phys. 54, p. 2093 (1983).

[24] P. J. Price, Surf. Sci. 113, p. 199 (1982).

[25] S. Mori and T. Ando, Phys. Rev. B19, p. 6433 (1979).

[26] S. Mori and T. Ando, J. Phys. Soc. Japan 48(3), p. 865 (1980).

[27] H. Störmer, A. Gossard, W. Wiegmann, J. Van. Sci. Technol. 21(2), p. 507 (1982).

[28] K. Lee, M. S. Shur, T. J. Drumond and H. Morkoc, IEEE Trans. Electron Dev. 30, p.207 (1983).

[29] R. A. Giblin , E. F. Scherer and R. L. Wierich, IEEE, Trans. Elec. Dev., vol. ED-20, p. 404 (1973).

[30] C. S. Chang and H. R. Fetterman, Solid-State Electrons vol. 30, p. 481 (1987).

[31] K. Lee, M. S. Shur, T. J. Drummond, and H. Morkoc, IEEE Trans. Electron Devices, ED-31(1), p. 29 (1984).

[32] B. Odekirk, "A review of HEMT technology", OCATE Microwave Engineering Colloquium, 1987.

[33] G. K. Reeves and H. B. harrison, IEEE Electron Device Lett. EDL-3 (5), p. 111 (1982).

Appendices

Appendix I

```
CAAAAAAAAAAAAAAAAAAAAAAAAAAAAAAAAAAAAAAAAAAAAAAAAAAAAAA
C  THIS PROGRAM SOLVES 2DEG CONCENTRATION
CAAAAAAAAAAAAAAAAAAAAAAAAAAAAAAAAAAAAAAAAAAAAAAAAAAAAAA
C
C ----- DEFINE  CONSTANT -----
C
      REAL    MO,EPSIL,DEC,MGAM,MDE,K,H,PI,Q,NC,OB,ED,EPS,
     +        DI,G,N,TP,LTP,EFI,EF2,Y,DELTA,NS,ND,NS1,ND1,ND2,X
     +        ,VW2,TP2,E0,E1
      REAL    NS2(100,5)
      INTEGER T,DII,MC
C
C ----- INPUT  PARAMETER -----
C
      F(X) = SQRT(2.*EPSIL*ND/Q*(DEC-X-EF2+DELTA)+(ND*DI)**2.)-ND*DI
      OPEN(2,FILE='DATA')
C     PRINT *, 'WHAT IS THE MOLE FRACTION'
C     READ *,X
C     PRINT *, 'WHAT IS THE SPACER LAYER THICKNESS IN A'
C     READ *,DII
C     PRINT *, 'WHAT IS THE TEMPERATURE'
C     READ *,T
C     PRINT *, 'WHAT IS THE THE DOPING CONCETRATION IN AlGaAs'
C     PRINT *, 'FROM'
C     READ *,ND1
C     PRINT *, 'TO'
C     READ *,ND2
C
C ----- PHYSICAL  PARAMETER -----
C
      X     = 0.3
      T     = 300
      ND1   = 1E17
      ND2   = 3E18
      MO    = 9.11E-31
      EPSIL = (13.1-3.*X)*8.85418E-14
      DEC   = .85*(1.247*X)
      MGAM  = .067+0.083*X
      MDE   = MGAM*MO
      K     = 1.38066E-23
      H     = 6.63E-34
      MC    = 1
      PI    = 3.141592
      Q     = 1.6E-19
      NC    = 2.*(2.*PI*(MDE/H)*(K/H)*T)**(3./2.)
      NC    = NC*.000001
      OB    = 1.
```

```
      ED     = (707*X-146)*.001
      DO  2 J=1,50
      ND     =(ND2-ND1)/50.*J+ND1
      DO  3 L=1,4
C
C ----- CALCULATION  NSO -----
C
      ITER   = 0
      EFI1   = -DEC
      G      = 2
      DI     = 30.*1.E-8*(L-1)
      G      = G*EXP(ED*Q/(K*T))
      N      = ND/NC
      TP     = -(1.-N/4.)+SQRT((1.-N/4.)**2.+4.*G*N)
      LTP    = TP/(2.*G)
      Y      = LTP
      VW2    = (K*T/Q)*LOG(LTP)
      EF2    = -VW2
      DELTA  = -(K*T/Q)*(LOG(1.+G*Y)+4./N*(LOG(1.-Y/4.)))
      EFI    = EFI1
      IMAX   = 20000
      EPS    = 0.1
 1    EFI    = EFI+ 0.001
      TP2    = ((2.*EPSIL*ND/Q)*(DEC+DELTA-EF2-EFI)+(ND*DI)**2.)
      IF ( TP2 .LT. 0. ) THEN
        GO TO 1
      END IF
      NS     = F(EFI)
      E0     = 2.5E-12*(100.**(4./3.))*NS**(2./3.)
      E1     = 3.2E-12*(100.**(4./3.))*NS**(2./3.)
      NS1    = 3.24E17*1.E-4*K*T/Q*LOG((1.+EXP((Q*EFI-Q*E0)/K/T))*
     +         (1.+EXP((Q*EFI-Q*E1)/K/T)))
      IF (ABS(NS-NS1)  .GE. (EPS*NS) ) THEN
        ITER = ITER + 1
        IF (ITER .GE. IMAX) THEN
C         PRINT *, 'METHOD DID NOT CONVERSE WITHIN LIMIT'
          PRINT *, ITER,EFI,F(EFI),NS1
          GO TO 4
        ELSE
          GO TO 1
        END IF
      ELSE
C       PRINT *,'METHOD HAS CONVERSED'
C       PRINT *,EFI,NS,ND
        NS2(J,L)  = NS
C       PRINT *, NS
      END IF
 3    CONTINUE
        WRITE  (2,*)  ND,NS2(J,1),NS2(J,2),NS2(J,3),NS2(J,4),NS2(J,5)
 2    CONTINUE
 4    STOP
      END
```

Appendix II

```
CAAAAAAAAAAAAAAAAAAAAAAAAAAAAAAAAAAAAAAAAAAAAAAAAAAAAAA
C  THIS PROGRAM SOLVES ONE-DIMENSIONAL GIBLIN MODEL OF HEMT (I-V)
CAAAAAAAAAAAAAAAAAAAAAAAAAAAAAAAAAAAAAAAAAAAAAAAAAAAAAA
      PROGRAM HEMTIV
C
C ----- DEFINE  CONSTANT -----
C
       COMMON ID,VG,VTO,GO,RS,RD,TO,TL,F,VS,U,L,VD,VDS,IDS,I1
      EXTERNAL FUNC,INTEG,NEWTON
       REAL     EPSIL,DEC,Q,OB,ND,DI1,DI2,RS,RD,VS,U,GO,VTO
      +         ,A,DEFI,F,VG,TO,TL,Z,L,ID,ID1
        REAL      ID2(50,4),VDS(4),IDS(4)
       INTEGER  T,I1
C
C ----- INPUT  PARAMETER -----
C
        OPEN(11,FILE='DATA2')
C       PRINT *, 'WHAT IS THE MOLE FRACTION'
C      READ *,X
C       PRINT *, 'WHAT IS THE SPACER LAYER THICKNESS IN A'
C       READ *,DI1
C        PRINT *, 'WHAT IS THE AlGaAs THICKNESS IN A'
C       READ *,DI2
C       PRINT *, 'WHAT IS THE TEMPERATURE'
C      READ *,T
C       PRINT *, 'WHAT IS THE THE DOPING CONCETRATION IN AlGaAs'
C      READ *,ND
      PRINT *, 'WHAT IS THE GATE LENGTH IN U'
      READ *,L
C       PRINT *, 'WHAT IS THE GATE WIDTH IN U'
C      READ *,Z
      PRINT *, 'WHAT IS THE THRESHOLD VOLTAGE'
      READ *,VTO
      PRINT *, 'WHAT IS THE MOBILITY'
      READ *,U
      PRINT *, 'WHAT IS GO'
      READ *,GO
      PRINT *, 'WHAT IS SATURATION VELOCITY'
      READ *,VS
      PRINT *, 'WHAT IS THE RS'
      READ *,RS
      PRINT *, 'WHAT IS THE RD'
      READ *,RD
C      PRINT *, 'WHAT IS THE GATE VOLTAGE'
```

```
C    READ *,VG
C
C ----- PHYSICAL PARAMETER -----
C
     X    = 0.25
     DII  = 30.
     DI2  = 600.
     T    = 300
     ND   = 2.E18
C     L   = 1.
     Z   = 50.
      EPSIL  = (13.1-3.*X)*8.85418E-14
     DEC    = .85*(1.247*X)
     Q      = 1.6E-19
     OB     = 1.09
     A      = 0.125E-16
C     VS    = 1.E7
C     U     = 4800.
C     RS    = 10.
C     RD    = 10.
     IF ( T .GE. 77 ) THEN
       DEFI = 0
     ELSE
       DEFI = 0.025
     END IF
C
C ----- CALCULATION  I-V -----
C
     Z     = Z*1.E-4
     L     = L*1.E-4
     DII   = DII*1.E-8
     DI2   = DI2*1.E-8
C     GO     = EPSIL*Z*VS/((DII+DI2)+EPSIL*A/Q)
C     VTO    = OB-DEC+DEFI-Q*ND*DI2**2./(2.*EPSIL)
      VDS(1) = 100000.
      VDS(2) = 100000.
      VDS(3) = 100000.
      VDS(4) = 100000.
C
C ----- SET INITIAL VALUE -----
C
     DO 50 I  = 1,20
       IF (I .EQ. 1) THEN
         ID1 = 1.E-6
       ELSE
         ID1 = ID2(I-1,1)
       END IF
C
C--- NEWTON METHOD -----
C
       DO 40 I1 = 1,3
         VG = 0.5*I1-2.0
```

```
        IF (VG .LE. VTO) THEN
           ID2(I,I1) = 0
          GO TO 40
        END IF
         IF (I .NE.1) THEN
            ID1 = ID2(I-1,I1)
        END IF
        ID = ID1
         VD = 0.1*I+0.
         IF (VD .GE. VDS(I1)) THEN
            ID = ID2(I-1,I1)
          GO TO 90
        END IF
         IF (ID .EQ.0) THEN
          GO TO 40
        END IF
        CALL NEWTON
         IF (ID .LE.1.E-6) THEN
          VDS(I1) = VD
            IDS(I1) = ID2(I-1,I1)
             ID2(I,I1) = ID2(I-1,I1)
          GO TO 40
        END IF
        GO TO 60
C
C ---- CHECK  OVERSATURATION -----
C
 90         IF (ID2(I-1,I1) .GT. IDS(I1)) THEN
             ID = ID2(I-1,I1)
        END IF
 60      ID1      = ID
         ID2(I,I1) = ID
C           WRITE(*,*) ID,'IDS(',I1,')=',IDS(I1),VDS(I1)
 40    CONTINUE
          WRITE  (11,101)  VD,ID2(I,1),ID2(I,2),ID2(I,3),ID2(I,4)
  101     FORMAT('',1F3.1,4F8.6)
          WRITE  (*,102)  VD,ID2(I,1),ID2(I,2),ID2(I,3),ID2(I,4)
  102     FORMAT('',1F3.1,4F9.6)
 50  CONTINUE
     STOP
     END
C
C ----- SUBROUTINE :NEWTON METHOD
C
     SUBROUTINE NEWTON
     EXTERNAL INTEG,FUNC
      COMMON ID,VG,VTO,GO,RS,RD,TO,TL,F,VS,U,L,VD,VDS,IDS,I1
      REAL FX,DFX,TEMP1,TEMP2,TO,TL,ID,GO,VG,VTO,RS,RD,F,VS,U,L,VD
       REAL VDS(4),IDS(4)
     INTEGER I
C
C -----  CALCULATION  ----
```

```
C
      I    = 0
      TEMP1 = VG-VTO-ID*RS
      TEMP2 = VG-VTO-VD+ID*RS
       IF (TEMP1 .EQ.0 ) THEN
         ID = 0
         GO TO 3
      END IF
       IF (TEMP2 .EQ.0) THEN
         ID = 0
         GO TO 3
      END IF
 10   TO   = ID/(GO*(VG-VTO-ID*RS))
      IF (TO .EQ. 0) THEN
         ID = 0
         GO TO 3
      END IF
      TL   = ID/(GO*(VG-VTO-VD+ID*RD))
      IF (TL .EQ. 0) THEN
         ID = 0
         GO TO 3
      END IF
      IF (TL .GE. 1) THEN
         VDS(I1) = VD
         IDS(I1) = ID
         GO TO 3
      END IF
       CALL INTEG(TO,TL,10,FUNC,F)
      FX   = ID*F+VS*L*GO/U
      TEMP1= (ID*GO*RS+GO*(VG-VTO-ID*RS))/(GO*(VG-VTO-ID*RS))**2.
       TEMP2= (-ID*GO*RD+GO*(VG-VTO-VD-ID*RD))/(GO*(VG-VTO-VD+RD*ID))**2.
      TEMP11= TL**2.*LOG(1-TL)*TEMP2
       IF (TEMP11 .EQ.0) THEN
         ID = 0
         GO TO 3
      END IF
      TEMP12= TO**2.*LOG(1-TO)*TEMP1
       IF (TEMP12 .EQ.0) THEN
         ID  = 0
         GO TO 3
      END IF
       DFX  = F+ID*(1/(TL**2.*LOG(1-TL))*TEMP2)-
     +       ID*(1/(TO**2.*LOG(1-TO))*TEMP1)
      IF (ABS(DFX) . EQ . 0) THEN
         PRINT *, 'METHOD FAILED'
         ID  = 0
         GO TO 3
       ELSE IF(ABS(DFX) .LT. 1.E-6) THEN
         PRINT *, 'METHOD IS LIKELY DIVERSING'
         ID = 0
         GO TO 3
      END IF
```

```
      DX   = -FX/DFX
      ID   = ID+DX
      I    = I+1
       IF (I .GT.20000) THEN
        PRINT *, 'METHOD DID NOT CONVERSE WITH LIMIT'
        PRINT *,I,DX,ID,FX
        GO TO 3
       ELSE IF(ABS(DX).LT. 1E-7 )THEN
      ELSE
        GO TO 10
      END IF
  3   RETURN
      END
C
C ----- FUNCTION NEED TO BE INTEGRATED -----
C
      FUNCTION FUNC(Q)
      REAL Q,FUNC
       IF (Q .EQ.0) THEN
        Q = 1
        GO TO 4
      END IF
      TEMP3 = Q*Q*LOG(1.-Q)
       IF (TEMP3 .EQ. 0) THEN
        FUNC = 1e30
        GO TO 4
      END IF
       FUNC = 1./(Q*Q*LOG(1.-Q))
  4   RETURN
      END
C
C -----   SUBROUTINE: TRAPERZOIDAL RULE
C
      SUBROUTINE INTEG ( C,D,IMAX,FUNC,F)
      EXTERNAL FUNC
      REAL C,D,F,SUM,DX
      INTEGER IMAX,I,K,N
      I    = 0
      N    = 2**I
       IF ( ABS(D-1) .LT. 1.E-3) THEN
         F = 0.5*(D-C)*(FUNC(C)+0.0)
      ELSE
         F = 0.5*(D-C)*(FUNC(C)+FUNC(D))
      END IF
C
C ----- INCREMENT THE ORDER -----
C
  1   I    = I+1
      IF (I .LE. IMAX)THEN
       N = 2**I
        DX= (D-C)/N
       K = 1
```

```
      SUM =0
2        IF( ABS((C+K*DX)-1) .LE. 1.E-3) THEN
           SUM = SUM + 0.0
      ELSE
         SUM = SUM + FUNC(C+K*DX)
       END IF
       K= K+2
     IF (K .LE. N-1)GO TO 2
      F= 0.5*F+DX*SUM
      GO TO 1
    ELSE
    END IF
    RETURN
    END
```